Utilization of High Throughput CRISPR Knockout Technologies to Identify Cellular Genes Involved in Human Papillomavirus Degradation of p53

Utilization of High Throughput CRISPR Knockout Technologies to Identify Cellular Genes Involved in Human Papillomavirus Degradation of p53

Erin M Lilienthal

A Thesis in the Field of Biology

for the Degree of Master of Liberal Arts in Extension Studies

Harvard University

May 2022

Abstract

High-risk human papillomaviruses (hrHPVs) are the causative agents for most cases of cervical cancer; they have also been linked to other anogenital cancers as well as head and neck cancers. Vaccines against HPV were introduced in the mid-2000s, and while they are effective at preventing new HPV infection, they do nothing to help the tens of millions of people currently infected with hrHPV and are not readily available in certain parts of the world. High-risk HPVs encode two oncoproteins – E6 and E7 – which target the cellular tumor suppressors p53 and Rb respectively. E6 works with other cellular proteins to ubiquitylate the cellular tumor suppressor p53, effectively marking it for degradation by the proteosome. Inhibiting E6-mediated ubiquitylation of p53 in HPV positive cervical cancer cells leads to p53 stabilization. Since HPV positive cancers express wild type p53, restoration of p53 triggers cells to undergo apoptosis. To address the need for novel therapeutics to treat HPV-induced cancers, we designed a functional genomics screen to identify cellular genes that are involved in hrHPV E6-mediated degradation of p53 in cervical cancer cells. Utilizing clustered regulatory interspaced short palindromic repeats (CRISPR)/ Cas9 technology, we screened over 8,000 cellular genes to identify those that, when knocked out, stabilized p53. This screen led to the identification of cellular targets, both previously identified and novel, that contribute to p53 degradation in HPV positive cells. We are hopeful these findings will provide potential therapeutic targets for HPV-induced cancers.

Dedication

I'd like to dedicate my work to my husband, Oskar Lilienthal, for his unconditional love and support. It was his kindness and compassion that enabled me to focus and pour all my energy into this work. Thank you, Oskar, for believing in me even before I believed in myself. I appreciate all that you've done to support our family and I hope to return the favor.

Acknowledgments

Throughout the process of conducting this project I have received a great deal of support and assistance. I would like to thank everyone involved in the success of this project and those who supported me outside of the lab as well.

I would like to acknowledge my thesis directors, Dr. Jennifer Smith and Dr. Peter Howley. Thank you, Peter, for welcoming me into your lab and entrusting me with this project, this experience and all that I have learned has been invaluable. Thank you, Jen, for your continued support and mentorship. You have challenged me to push beyond what I thought was impossible and provided everything I needed to be successful.

I would also like to thank my coworkers at the ICCB-L screening facility. Thank you, Jen Splaine and Dave Wrobel, for your help with data curation and analysis. Thank you, Clarence Yapp, for your help developing acquisition and analysis protocols on the IXM-C. A special thanks to Richard Siu and Alasdair Morton for their help with the project but also their friendship and support; I appreciate all that you've both taken on so I could focus on this thesis.

In addition, I would like to thank all the lab members in the Howley Lab: Rebecca Kramer, Asma Sheikh, Gustavo Martínez-Noël, and Patricia Szajner for their insights, conversations, support, and friendship throughout this process.

Finally, I would like to thank my family and friends for all their support. In particular I'd like to thank my mom who hosted me for writers retreats and lent a sympathetic ear whenever I needed her.

Table of Contents

List of Tables

List of Figures

Chapter I.

Introduction

Human Papillomavirus

Human papillomavirus (HPV) is the most common sexually transmitted infection in the world. More than 42 million Americans are currently infected with different HPV types and approximately 13 million Americans are being infected each year (CDC, 2021). Papillomaviruses are classified by and restricted to their host species. They are typed by their DNA sequence similarities and over 200 different HPV types are currently identified (Howley, P., 2021). High-risk HPVs (hrHPVs) are those associated with the development of cervical cancer, with HPV16 being the most common cancer-associated type and HPV18 a close second.

HPVs are small, around 60nm in diameter, and icosahedral in shape; they contain double stranded circular DNA that replicate in the nuclei of squamous epithelial cells (Howley, P., 2021). There are ten translation open reading frames (ORFs), all located on one strand of viral DNA. HPV ORFs are classified as either early (E) or late (L) based on their location and encode viral regulatory and capsid proteins respectively (Howley, P., 2021). High risk HPVs encode two viral oncoproteins – E6 and E7 – that are expressed in hrHPV associated cancers. Conserved regions on the E7 protein from hrHPV are responsible for binding important cellular regulatory proteins including cyclin-dependent kinase inhibitors. The product of the retinoblastoma tumor suppressor gene, pRB, in its hypophosphorylated form is active and inhibits cell cycle progression. hrHPV E7 binds

hypophosphorylated pRB, essentially sequestering it and enabling the cell cycle to continue (Howley, P., 2021). The lack of cell cycle regulation typically leads to increased levels of the tumor suppressor protein p53. Since there is no selective pressure for p53 mutations in HPV cancers, cells express the wild type (WT), proapoptotic p53. E6 is utilized by hrHPV-infected cells to prevent apoptosis; the oncoprotein forms a complex with the cellular ubiquitin-protein ligase UBE3A, or E6-associated protein (E6AP), a protein that is responsible for directly transferring ubiquitin to its substrate. E7 inhibition of pRB function results in DNA replication stress that stabilizes p53. E6 in turn targets the ubiquitin mediated degradation of p53, relieving the p53 check point block and allowing the cells to proliferate (Scheffner, M., 1993). E6 blocks the transcriptional function of p53 and effectively inhibits DNA damage and oncogene-mediated cell death signals, causing antiapoptotic activities and interfering with cell cycle regulatory functions of p53. The expression and activities of hrHPV E6 and E7 in HPV+ cells promote continuous replication.

The long control region (LCR) is around 1 kilobase in size and does not have any ORFs; instead, it encodes for the origin of DNA replication and important transcription control elements. The LCR contains enhancer elements that respond to cellular factors involved in differentiation. Viral proteins E6 and E7 are transcribed from a promoter found within the LCR, and the papillomavirus E2 protein was found to be capable of repressing the LCR (Dowhanick, J. J., 1995). The HPV E2 protein is well conserved among papillomaviruses and has known regulatory functions affecting viral transcription and DNA replication as well as long-term plasmid maintenance (Howley, P., 2021). E2 proteins bind E2-specific sites in promoter regions of the viral genome. E2-mediated

repression of the E6 and E7 promoters are required to induce growth arrest of HeLa cells (Francis, D. A., 2000). Repression of E6 and E7 genes results in the reactivation of p53 and Rb pathways, inducing cell cycle arrest and cellular senescence.

HPV Vaccines

The HPV vaccine Gardasil® was first approved by the FDA in 2006 and Gardasil®9 was approved in 2014. Since 2017, Gardasil®9 is the only HPV vaccine available in the US (KFF, 2021). Beginning in 2015, the World Health Organization (WHO) recommends two doses of HPV vaccine at either a six month or one year interval and the original three-vaccine schedule for those 15 and older (Harper, D. M., 2017). There is also a one dose vaccine available called Cervarix, offering an easier and more economical vaccination program for low-income countries. In high income countries, a seven-year follow-up study showed that when vaccination rates exceed 50%, HPV16 and HPV18 infections decreased by 64%. The same success has not been observed from a global perspective, particularly in economically repressed countries (Harper, D. M., 2017). Vaccination against HPV cannot replace the need for screening in the prevention of cervical cancer because of the number of people currently infected with hrHPV and the continued high rates of new infection. Vaccines are an essential preventative measure to stop HPV infection in vaccinated individuals, however, they have no therapeutic value to those already infected. Considering vaccination efforts are not reaching a more global population and do nothing for those already infected, another line of defense is needed to prevent HPV-induced cancers.

HPV and Cancer

There are around 530,000 women worldwide newly diagnosed with cervical cancer each year and more than 350,000 of these cases are diagnosed in less developed countries (de Martel C et al., 2017). The Papanicolaou test, also known as a pap smear, screens for cervical cancer and has proven to be effective at decreasing the frequency of hrHPV infections that progress to cervical cancer in industrialized nations. The privilege of routine cervical cancer screening is not readily available in all areas of the world. Women in some areas are dying of a preventable disease due to the high cost of cytologic screening and challenges of the HPV vaccine. Nearly all cervical cancers (99.9%) contain hrHPV DNA and these viruses are attributable for around 5% of cancer in humans worldwide (de Martel, C., 2020). Other HPV-related cancers include oropharyngeal cancers, anal cancer, penile cancer, vaginal cancer, and vulvar cancer (National Cancer Institute, 2021). Anyone infected with hrHPV is at risk of developing cancer.

High Throughput Screening Efforts to Elucidate the Role of HPV in Cancer

High throughput screening is a powerful experimental strategy to identify cellular genes and compounds that affect various aspects of many biological processes including viral replication cycles. When designed and optimized correctly, high throughput assays allow hundreds or thousands of individual experiments to be conducted simultaneously in each well of a microplate. This facilitates the screening of entire genomes or large compound libraries, enabling hypotheses to be generated and future research to focus on

a smaller subset of genes or small molecules with true potential to address the research questions at hand.

Both functional genomic and small molecule screens have proven informative in the context of HPV. The Howley Lab is experienced in utilizing high throughput screens to determine the cellular proteins that are involved in the HPV oncogenic potential. A genome-wide siRNA screen identified 96 cellular genes that contribute to the ability of hrHPV E2 to transcriptionally repress the LCR, a region of the viral DNA that directs expression of both E6 and E7 (Smith, J. A., 2010). A live-cell high content small molecule screen enabled Martínez-Noël and colleagues to identify compounds that stabilize p53 over time (Martínez-Noël, 2021). A high throughput screen of miRNA mimics identified classes of miRNAs that impact the ability of E6 and E6AP to degrade p53 in HPV+ cervical cancer cells (Martínez-Noël, 2022). In addition, members of the Howley Lab have conducted a full-genome siRNA screen to identify cellular proteins involved in E6/E6AP-mediated degradation of p53 (Martínez-Noël, unpublished).

Other groups have also utilized high throughput screens in search of identifying compounds with therapeutic potential against HPV-related cancers. Kalu and colleagues screened 1062 unique compounds at six different concentrations in 24 cell lines to identify compounds that induce cell death in HPV-associated head and neck cancers (Kalu, N. N., 2016). The same group then looked at head and neck cancers, as well as cervical cancers, and conducted a high-throughput drug screen of 1122 compounds (Kalu, N. N., 2018). The latter study compared drug sensitivity in HPV-positive and HPV-negative cell lines. Another group engineered full-length HPV genomes that express reporter genes to screen for inhibitors of hrHPV replication. They were

successful in identifying five HPV replication inhibitors that could serve as promising candidates for HPV antivirals (Toots, M., 2017).

CRISPR Cas9

CRISPR, which stands for clustered regularly interspaced short palindromic repeats, was originally discovered as a defense mechanism for bacteria against invading viruses and plasmids (Sternberg, S. H., 2014). This technology has become a powerful tool for genome editing. It enables researchers to selectively knock out, silence, knock in, and modify target genes of interest (Nidhi, S., 2021). CRISPR Cas9 knockout requires a single guide RNA (sgRNA) that is synthetically made to contain two components: CRISPR RNAs (crRNA) and trans-activating crRNA (tracrRNA) that associate via base pairing. The crRNA contains a 20-nucleotide sequence that is complementary to the target gene and the tracrRNA acts as a scaffold, promoting sgRNA association with the Crispr Associated (Cas) enzyme (Jinek, M., 2012). The sgRNA/Cas complex is directed to a trinucleotide protospacer adjacent motif (PAM) that is adjacent to the target gene's sequence. Once bound, Cas9 cleaves both strands of DNA three nucleotides upstream of the PAM, generating a double-strand break (DSB) (Sternberg, S. H., 2014). The DSB is then attempted to be repaired by host-mediated DNA repair mechanisms, but nonhomologous end joining (NHEJ) is error prone. NHEJ employed by the host creates random insertions, deletions and or substitutions at the DSB site, effectively knocking out the target gene specified by the sgRNA (Jiang, F., 2017). A variety of different techniques facilitate the use of CRISPR Cas9 technologies in mammalian cells. They

range from physical manipulation including electroporation and microinjection to viral or lipid nanoparticle-mediated delivery.

CRISPR Technologies in High Throughput Screening

The introduction of CRISPR technologies to high throughput screening provided investigators with a novel approach to not just decrease or knock-down, but fully knock out target genes. RNA interference, specifically siRNA and shRNA, has been an invaluable tool for loss-of-function screening (Agrotis, A., 2015), however the technology is not without critics, as knock down is not the same as knock out and there is the potential for miRNA-like off-target effects (Wang, F., 2018). CRISPR allows for a complete knock out of target genes, selectively eliminating target protein levels with little to no off-target effects. As CRISPR methods continue to be optimized, they may surpass the current siRNA-based approaches to become the primary high-content screening method (Agrotis, A., 2015).

The expansion of CRISPR technologies into a HTS platform allows for thousands of genes to be interrogated simultaneously either in a pooled or arrayed approach. While initial pooled approaches relied on both Cas9 and sgRNA transduction via lentivirus, scientists quickly adapted a strategy of sgRNA lentiviral transduction into mammalian cells already expressing the Cas nuclease. Cells are infected at a low multiplicity of infection to ensure one sgRNA per cell and then undergo antibiotic selection for sgRNA transduction. Cells are allowed to replicate, and the phenotype of interest is selected. Pooled CRISPR screens typically take about two weeks of cell culture and rely on next-

generation sequencing to quantify the changes in sgRNA between the phenotype of interest and starting cell population (Agrotis, A., 2015).

High throughput CRISPR arrayed screening has the advantage of utilizing optimized methods for reagent delivery and automated instrumentation already developed and utilized for siRNA screening. Arrayed libraries are in microplate format with a unique virus vector, plasmid, or sgRNA preparation in each well targeting one gene/well (Agrotis, A., 2015). Cells are grown in microplates and can either express the Cas9 enzyme or have Cas9 mRNA or protein co-delivered with sgRNA. The use of cells with stable or inducible Cas9 expression can be advantageous because it is relatively easy to work with, but Cas9 expression may introduce phenotypic artifacts, have variable levels of expression, or not be compatible with all cell types (Agrotis, A., 2015). Co-delivery of Cas9 mRNA or protein alleviates any deleterious effects of stable Cas9 expression, but is more expensive and challenging, especially in high-throughput format. In contrast to pooled screens, there are no selection steps for sgRNA-mediated arrayed CRISPR screens.

This project utilized libraries of arrayed sgRNA in a one-gene per well format. An arrayed screen requires phenotypes to be identified but not selected for, allowing multiple phenotypes to be investigated simultaneously (Agrotis, A., 2015). The phenotypic readout of the assay should produce wells containing positives or “hits” with a clear signal increase or change from what is considered background. The positive and background signal must also be consistent with little variance to have confidence in the hit calling criteria. Each well containing different genes that were knocked out via CRISPR/Cas9 transfection can then be analyzed for their individual ability to produce a

phenotypic response or signal in comparison to the controls built into the assay. While selection is not possible utilizing an arrayed approach, it does allow for the roles of essential genes and secreted proteins to be examined and eliminates the need for sequencing.

Significance

This arrayed high throughput CRISPR screen is the first to be designed, conducted, and completed at the ICCB-Longwood Screening Facility at Harvard Medical School. The assay development and optimization for this screen will provide fundamental knowledge to help inform the optimization efforts for future high throughput arrayed CRISPR screens. While other similar screens have been conducted, nearly all published efforts were in 96-well format. They are not miniaturized or automated to the same extent as the screen described here. This research can provide those wanting to develop a similar screen with a strong foundation to not only benchmark assay parameters, but also what to expect in terms of phenotypic response, data analysis, etc.

Vaccines have proven to be useful tools in the prevention of HPV infection, but they only help prevent infection and are not readily available throughout the world (Toots, M., 2017). Since the vaccines were not available until the mid-2000s, there are millions of people infected with hrHPV prior to 2005 and are at risk for HPV-associated cancers. There is no current method to fully irradicate HPV, meaning there will always be a need for therapeutics to prevent an infection from becoming cancerous. The goal of this screen is to identify cellular genes that play a role in HPV E6-mediated degradation of

p53 in HPV18 positive cervical cancer cells. Taken together, the results from this study will help identify cellular genes that result in the stabilization of the p53 protein in HPV+ cervical cancer cells.

Chapter II.

Materials and Methods

Engineering Cell Line and Culture Practices

HPV18+ HeLa cells were engineered to express inducible Cas9 (iCas9) protein fused to enhanced green fluorescent protein (eGFP) (Cao, J., 2016) and mutant R273C p53 protein fused to mRuby fluorescent protein (Howley Plasmid #7677). The maps of the iCas9-eGFP and R273C p53-mRuby plasmids used are included in Figure 1. Cells were transduced using a virus containing the mutant R273C p53-mRuby plasmid and were selected under 650.8μM neomycin (ThermoFisher, 21810031) treatment for one week. They were then treated with 500nM of Bortezomib (Millipore Sigma, 5043140001) for 24h to induce p53 stabilization and subsequent mRuby accumulation. Cells were sorted for the presence of mRuby (stabilized p53) via BD Bioscience's fluorescence-activated cell sorting (FACS) machine (FACSAria™ Cell Sorter). Cells were then transduced with a second plasmid, Lenti-iCas9-neo, which was a gift from Qin Yan (Addgene plasmid # 85400; http://n2t.net/addgene:85400; RRID:Addgene_85400) (Cao, J., 2016). After neomycin-mediated selection using the same conditions, cells were then induced with 1.95μM of doxycycline hyclate (dox) (Sigma-Aldrich, D9891-5G) for 24 hours to induce Cas9 expression and produce GFP signal. Cells were sorted on the FACS machine again four times for GFP fluorescence and twice for the absence of mRuby fluorescence. Subsequently, cells were cultured for one week to enable silencing

of the promoter driving Cas9 and were sorted again for no GFP and no mRuby fluorescence. Aliquots of cells were cryopreserved in liquid nitrogen, with new aliquots thawed after approximately 15-20 passages. This was done to ensure the expression of Cas9 and R273Cp53-mRuby were not silenced over time. Cells were cultured in hgDMEM (ThermoFisher, 11995073) and 10% filtered, fetal bovine serum (FBS) (ThermoFisher, 26140079), with twice weekly passaging at approximately 80% confluence. For Cas9 induction, cells were treated with doxycycline (dox) at a final concentration of 5.85μM 24 to 48h prior to transfection.

Screening Synthego's sgRNA Human Druggable Genome Library

Synthego's arrayed, synthetic single guide (sg)RNA CRISPR knock out library was screened at the ICCB-L Screening Facility at Harvard Medical School. There were 29 384-well plates comprised of 8,478 different sgRNAs stored in TE buffer (10mM Tris-HCl, 1mM EDTA, pH 8.0) at a final stock concentration of 1μM. The design was based on Gencode Release 26 (GRCH38.p10) (GENCODE, 2021) and utilized algorithms to minimize off-target effects and enhance the likelihood of fragment deletion to generate a full knock out.

Each library plate contained controls in column 12, three wells of each essential (COPA and KIF11) and non-essential (NLRP5 and KRT77) gene target. A control plate was prepared for each transfection appointment so that assay-specific positive and negative controls could be added to assay plates with the same automation as the library sgRNAs. All sgRNA were purchased from Synthego and diluted according to

manufacturer's rehydration protocol. Guides were rehydrated to 5uM using 1x TE buffer (Thomas Scientific, C751A72) and concentration verified using a nanodrop, then stored at -80°C. The sgRNA pools were freshly diluted to 1uM to be plated in the control plate (Eppendorf, 951020729) prior to transfection. The death inducing KIF11 essential gene served as a positive transfection control, and the non-essential NLRP5 gene served as a negative control for p53 stabilization. The PSMA4 and PSMA2 multi-guide sgRNA were utilized as weak and strong positive controls, respectively.

At 48 hours prior to transfection, Cas9 expression was induced with 5.85µM of dox; induction was visually confirmed prior to transfection. Each library plate was screened in technical triplicate and all replicate plates were labeled with the corresponding library plate number and replicate letter. The order of plates was maintained throughout each step, ensuring the timing of each addition step was consistent. RNAiMAX (ThermoFisher, 13778150) was diluted in OptiMEM (ThermoFisher, 31985070) to result in 0.2% of the final well volume. Using a Thermo MultiDrop Combi, 9µL of OptiMEM (8.9µL)/RNAiMAX (0.1µL) was added to each well of a black-walled, clear-bottom, tissue-culture treated 384-well microplate (Corning #3764). Plates were briefly centrifuged, then 1.25µL of 1µM sgRNA was added to each well with an Agilent Bravo, resulting in a final concentration of 25nM. Well contents were mixed up and down three times. Cells were trypsinized and resuspended into a single-cell suspension with media containing 12.5% FBS and 5.85µM of dox, then diluted to $1.5e^4$ cells/mL. After a minimum of 20 minutes, which enabled the lipid and sgRNA to complex, 40µL of cell suspension was seeded on top of the transfection reaction mixture using a Combi. The plating density was 600 cells/well, the final

concentration of sgRNA was 25nM, and the total well volume was 50.25µL. Microplates were briefly centrifuged and incubated at room temperature (RT) for 20 minutes on a flat surface prior to being placed in the incubator at 37ºC, 5% CO_2 for 96h.

Fixation and Staining

Plates were removed from the incubator and media aspirated using a stainless steel, 24-channel aspiration wand (Drummond, 300001). The aspiration wand was modified so 15µL of liquid remained at the bottom of the wells to avoid disruption of the cell monolayer. Using the Combi, 50µL of filtered, 1x phosphate buffered saline (PBS) (Corning, 46-013-CM) was added to each well. The PBS was aspirated and 30µL/well of 6% paraformaldehyde (PFA) (VWR, 97064-888) and 1:1500 dilution of Hoechst 33342 Solution (Invitrogen, H3570) diluted in 1x PBS was added to each microplate. Plates were incubated at RT for 20 minutes, then washed three times with 50µL/well of 1x PBS. After the final wash, 50µL of 1x PBS was added to each well to prevent the cells from drying out and reduce background interference during image acquisition. Plates were sealed with AbsorbMax black seals (BK-50). Any plates not immediately imaged were stored at 4ºC. Figure 2 depicts the screening workflow including fixation and staining steps.

Image Acquisition and Analysis

Immediately prior to image acquisition, the bottoms of each plate were cleaned with 70% ethanol, kimwipes, and microfiber cloths to ensure no dust particles or

smudges were on the bottom of the plate. Images were acquired on Molecular Devices' ImageXpress Micro Confocal (IXM-C) Laser Microscope. A 10x magnification objective was utilized to image one site in the center of each well, excluding the perimeter and capturing 32.2% of the well. The 405nm excitation filter and 452/45nm emission filter set for the DAPI channel and 546nm excitation filter and 595/31nm emission filter for the TRITC channel were utilized to acquire the Hoechst and mRuby fluorescent signals, respectively. The exposure time for the DAPI channel was set to 2ms and the TRITC channel was set to 1ms. The focus offset was checked prior to each run and was only adjusted in miniscule increments if the resulting image was not optimally focused.

A custom analysis module was created using Molecular Devices' MetaXpress software to quantitate number of nuclei in each well using the Hoechst fluorescent signal and typical shape and size of the nuclei parameters of approximate minimum width = 8.1µm, approximate maximum width = 24.51µm, and intensity above local background = 367. Another mask was created to quantitate number of p53+ nuclei based on mRuby fluorescent intensity (intensity above local background = 306) and size (approximate minimum width = 13.5µm, approximate maximum width = 36.82µm) to classify a mRuby+ cell. The total cell count and p53+ cell count was exported from MetaXpress to excel and a percentage of p53+ cells (mRuby+) was calculated for each plate.

Data Analysis

Assay-specific positive and negative controls, mentioned earlier and depicted in Figure 3, were included on every assay plate and a Z' factor (Zhang, J. H., 1999) was

calculated for each assay plate using PSMA2 as the positive control and NLRP5 for the negative control. The Z' factors ranged between 0.02 and 0.54 throughout the screen. Any plates whose Z' factors were < 0 were rescreened. The correlation of total nuclei and % p53+ cells was calculated between replicates for each library plate, using the R^2 value to measure linear correlation. Experimental wells that had ≥ 10% p53+ cells in at least two of the three replicates were considered potential positives for further confirmation. Wells that had at least 10% p53+ cells, but < 100 cells were flagged to be reviewed. All images of experimental positives were qualitatively evaluated to confirm the quantitative number provided by the analysis algorithm.

Chapter III.

Results

Image Acquisition and Analysis Optimization

HeLa cells stably transfected with mRuby-tagged R273Cp53 and doxycycline-induced Cas9 (Figure 1) were used for the development of a high throughput, phenotypic screen enabling quantitation of p53 stabilization. Initial effort was focused on optimization of cell plating densities and image acquisition and analysis. Several aspects had to be considered when determining the ideal plating density: incubation period of several days; requirement of subconfluent monolayers for accurate quantitation of cell number (Agrotis, A., 2015); and high enough initial cell density to prevent toxicity observed from transfection reagents (Wang, T., 2018). Densities ranging from 400 cells/well up to 4,000 cells/well were tested and the optimal plating cell density was determined to be 600 cells/well. This density allowed for ~80% confluency at the time of acquisition and resulted in minimal transfection-induced toxicity.

The total number of cells and number of mRuby-positive cells were quantitated in each well by staining nuclei with Hoechst and using the mRuby tag on p53. Initial image acquisition captured the entirety of each well on the 384-well microplate using the 4x magnification objective. Cells, visualized by their Hoechst-stained nuclei, tended to cluster in the periphery of each well, making MetaXpress's automated classification of single cells inaccurate. To improve analysis, the exterior area of each well was excluded

from the image by defining the acquisition site to the center of the well, capturing ~65% of the total area. Magnification was increased to 10x to increase resolution, still enabling >30% of the total well area to be captured.

The DAPI wavelength exposure time was optimized by acquiring images of wells containing cells with Hoechst-stained nuclei. An exposure time of 2ms produced fluorescent signal that was within the range of the microscope's detector, but not too bright where pixels became saturated. The TRITC wavelength exposure time, used to acquire the mRuby signal, was optimized in a similar fashion. Since initial assay development efforts were focused on image acquisition and analysis rather than transfection and CRISPR-mediated knock out, the proteasome inhibitor Bortezomib was used to stabilize p53 in the HPV18 positive HeLa cells (Martínez-Noël, 2021). It is documented that siRNA-mediated silencing of E6AP leads to the stabilization of p53 in HeLa cells (Kelley, M. L., 2005); this was also used as a positive control during assay development. The optimal exposure time for the TRITC wavelength was determined to be 1ms. Untreated wells were also analyzed to ensure the fluorescent signal was due to the expression of mRuby-p53. Figure 4 depicts total nuclei and stabilized p53 in cells following Bortezomib treatment (A&B) or siRNA-mediated knock down of E6AP (C&D) compared to non-treated cells (E&F).

Once the acquisition protocol was optimized, a custom image analysis module was created to count the total number of nuclei and p53 positive cells in each well. The algorithm used size exclusion and fluorescent thresholds to accurately count nuclei and p53 positive nuclei. Based on analysis of representative cells varying in size and fluorescent intensity, nuclei were defined between 8.1µM and 24.51µM wide and at least

367 fluorescent intensity units above background. The p53 positive nuclei were defined as having at least 306 fluorescent intensity units above background and were between 13.5µM and 36.82µM wide in size. To exclude small fluorescent artifacts in the TRITC channel and account for larger, senescent cells where fluorescent signal was present outside the nucleus (Green, D. R., 2009) the size selection criteria for p53+ cells was slightly larger than the criteria used for identifying nuclei.

Optimization of Cas9 Induction and sgRNA Transfection

Essential to the success of this high throughput screen were the doxycycline-induced kinetics of Cas9 expression. Cells were engineered to express Cas9 tagged with eGFP driven by a dox-inducible promoter. During cell line selection for Cas9+ cells, doxycycline was added 24h prior to sorting or transfection at a concentration of 1.95µM. Initial optimization efforts followed the same induction timing and concentration of dox prior to transfection. Later experiments demonstrated that cells tolerated a dox concentration of 5.85µM with no additional toxicity compared to the cells treated with 1.95µM. In addition, 48h of treatment (Figure 5B) significantly increased Cas9 expression when compared to 24h (Figure 5A). For the screen, cells were induced with 5.85µM of doxycycline 48h prior to transfection and media was supplemented with 5.85µM of doxycycline at the time of reverse transfection, effectively providing available Cas9 for up to 48h post transfection. On average, at least 75% of cells were Cas9 positive, as measured by eGFP expression, at the time of transfection (Figure 6).

siRNA and sgRNA targeting E6AP, the cellular E3 ligase that is essential for E6-mediated degradation of p53, were used to optimize an automated reverse transfection protocol. While there was a robust stabilization of p53 following E6AP knockdown with siRNA, evident in Figures 4 (C&D) and 7 (E&F), this was not observed post-transfection with the Synthego's sgRNA designed against E6AP (Figure 7 A, B, C, D, I, J, K, L). Several parameters including transfection reagent and concentration, cell density, incubation time, guide concentration, and dox induction were tested in an effort to increase the efficiency of sgRNA-mediated E6AP knock out. Three transfection reagents were tested (RNAiMAX, CRISPRMAX, and DharmaFECT1) at concentrations ranging from 0.2% - 1.6% of the total well volume. Tested cell densities ranged from 400 cells/well up to 4,000 cells/well and tested incubation periods ranged from 48h – 144h. Despite these efforts, p53 stabilization did not increase following E6AP sgRNA transfection (Figure 7).

A sgRNA targeting kinesin family member 11 (KIF11) was included in the optimization experiments as a measure of transfection efficiency. Depletion of KIF11, which plays an essential role in spindle dynamics during mitosis, is known to cause growth inhibition and non-apoptotic cell death in cancer cells (Martens-de Kemp, S. R., 2013). As expected, a dramatic decrease in cell number was observed following KIF11 sgRNA transfection, as illustrated in Figure 7O. Cells that were transfected with KIF11 sgRNA but lacked Cas9 induction via doxycycline addition displayed no decrease in cell number (data not shown). Taken together, these findings indicate that Cas9 induction is sufficient, and the reverse transfection is effective. Thus, it was hypothesized that the sgRNAs we tested targeting E6AP did not lead to its knockout in HeLa cells.

It is well documented that the proteasome is essential for E6-mediated degradation of p53 (Scheffner, M., 2003). To identify a positive control sgRNA for this assay, we asked whether transfection with a sgRNA targeting a proteasomal subunit would result in p53 stabilization. Synthego's human arrayed sgRNA CRISPR-Cas9 library was formatted in alphabetical order according to gene symbol, so all sgRNA targeting proteasomal subunits were included on a single library plate, #51510. This plate was screened in technical triplicate (Figure 8). Several of the sgRNAs led to a measurable stabilization of p53. Guides targeting proteasome subunit alpha type-2 and proteasome subunit alpha type-4 (PSMA2 and PSMA4) had an average of 25.1% and 15.6% p53+ cells respectively, a significant increase from non-essential control NLR Family Pyrin Domain Containing 5 (NLRP5) which averaged 0.1% of cells with stabilized p53. NLRP5 expression is restricted to the oocyte (NCBI, 2022), therefore no phenotypic response was expected or observed post transfection, rendering this guide an appropriate negative control for the assay. PSMA2 and PSMA4 both code for proteins on the proteasome's 20S subunit and were chosen to be strong and weak positive controls, respectively, helping to define the upper and lower limits of significant p53 stabilization (Figure 9).

Based upon all the above-described experiments, the following high throughput screening protocol was utilized: 5.85µM doxycycline induction 48h prior and during transfection; cell density of 600 cells/well; 0.2% RNAiMAX; final sgRNA concentration of 25nM; and a 96h incubation period post transfection. Guides targeting PSMA2 and PSMA4 were used as the positive controls for p53 stabilization, NLRP5 sgRNA functioned as the negative control, and sgRNA targeting KIF11 served as the positive

control for transfection efficiency. The final high throughput assay workflow is illustrated in Figure 2.

Primary Screen Results

Controls were checked on each plate prior to acquisition for p53 stabilization by acquiring a few wells and visually inspecting the image for the presence of mRuby signal. Once all plates were acquired and analyzed, a Z' factor was calculated on each assay plate using positive and negative control wells to assess the robustness of the assay throughout the screen (Zhang, J. H., 1999). Based on the results from the NLRP5 and PMSA2 wells, Z' factors ranged between 0.02 and 0.54. Cell density was also confirmed to be within 1,500 and 2,500 cells/well; any plates with total nuclei counts that fell outside this range were triaged and rescreened.

There were 52 genes that when knocked out, left less than 100 cells in each well across the three replicates. These potentially toxic guides are listed in Table 1. In addition to KIF11, there were four genes that when knocked out resulted in < 50 cells/well: HIST1H4C, RAN, VCP, and PLK1. Figure 10 depicts the low nuclei count of HIST1H4 (A), RAN (D), VCP (E), and PLK1 (C) relative to the non-essential NLRP5 control (B). Each of these genes are considered essential for cell or cancer cell survival due to their roles in cell cycle progression (HIST1H4C, VCP, PLK1) and DNA replication (RAN, VCP). VCP and PLK1 are considered potential cancer therapy targets because their inhibition has been shown to cause cell death in cancer cells (Liu, Z., Sun, 2016; Costantini, S., 2021).

Figure 9 depicts the average percent of p53+ cells across the three replicates on the Y-axis plotted against the corresponding Well ID. There was significant toxicity observed in the controls added to plates 51495-51498 due to diluting the controls in a toxic batch of TE buffer. This resulted in decreased p53 stabilization in the PSMA2 and PSMA4 controls indicated in dark green and light green, respectively. Throughout the screen, PSMA4 controls typically scored ≥ 10% and PSMA2 controls defined the higher range of expected p53+ cells, between 15 and 30%. The primary hit calling criteria was defined as any experimental well (indicated in grey) that had > 10% of cells with stabilized p53 in at least 2 out of the 3 replicates. This was considered a significant increase above background levels, which did not exceed > 1% p53+ cells/well.

Cells were engineered to express mutant R273C p53 in attempt to decrease apoptosis due to p53 stabilization. However, apoptosis was still an expected outcome because WT p53 was still expressed and stabilized along with R273C p53. Normalization to cell number decreased the impact of cell viability, but it is possible that wells with few cells could have had p53+ cells that had undergone apoptosis prior to imaging. For this reason, positive wells with low cell counts (≤ 100 total cells) were still included in the top hit list but were flagged due to their potential cellular toxicity.

To include potential positive wells that scored below 10% of p53+ cells but still had a significant number of cells with stabilized p53, any well that had >15 p53+ cells in at least 2 out of the 3 replicates were also considered a hit. Figure 11 plots the average % of p53+ cells against the total nuclei for all tested wells; the hits that scored positive using the ≥10% p53+ criteria, indicated in red, typically had lower cell counts compared to the hits that scored positive based on the number of p53+ cells, indicated in orange.

This is apparent looking at the distribution of red hits that were higher on the Y-axis but typically further to the left on the X-axis, indicating the ≥10% p53+ hits had lower cell counts relative to the >15 p53+ hits that were lower on the Y-axis and were further to the right on the X-axis. There were 77 genes that scored positive based on the ≥10% p53+ criteria and 75 genes that scored positive based on the >15 p53+ cells criteria. Plate 51510 was rescreened and all proteasomal subunits that scored positive from the initial validation screen reconfirmed.

Based on the above criteria, out of the 8,479 genes tested, a total of 152 scored positive for their ability to stabilize p53. A complete list of potential hits from the primary screen are included in Table 2. Many of the stronger potential hits with ≥ 20% p53+ or ≥ 40 p53+ cells were genes targeting proteasomal subunits. Out of the 37 proteasome genes tested, a total of 22 scored as potential positives for p53 stabilization. A total of 10 genes were reconfirmed from the whole genome siRNA screen that was previously conducted in the Howley Lab, eight of which were expected proteasomal subunit proteins: PSMA6, PSMB6, PSMD1, PSMD14, PSMC1, PSMD7, PSMD2, and PSMB4. The two other genes that scored positive in both screens were NDUFA6 and MAP3K9. Table 2 includes a column indicating whether each hit was tested in the siRNA screen and if that gene was positive or negative. Chromosomal segregation 1 like protein (CSE1L) had the largest average number of p53+ cells across the three replicates with an average of 71 p53+ cells. Karyopherin beta 1 (KPNB1) had the highest percentage of p53+ cells across the three replicates with an average of 37.2% p53+ cells. There were 13 genes with ≥ 20% p53 stabilization and 12 genes with ≥ 40 p53+ cells.

Chapter IV.

Discussion

Significance

Despite the development of vaccines that prevent hrHPV infection, there are minimal options to irradicate cells already infected with HPV (Howley, P., 2021). There is a need to elucidate which cellular genes aid hrHPV infection in its progression to cancer. Various types of high throughput screens have been developed and conducted in an effort to discover potential therapeutics or targets to treat HPV+ lesions. These include small molecule (Martínez-Noël, 2021; Kalu, N. N., 2016; Toots, M., 2017) and functional genomic screens via interrogation with siRNA (Smith, J. A., 2010; Martínez-Noël, unpublished) or miRNA (Martínez-Noël, 2022). Our goal is to conduct a high-throughput screen utilizing CRISPR Cas9 knockout technologies to identify cellular genes required for HPV E6-mediated degradation of p53. While the results of this screen are very promising, it is important to remember this research work is the completion of the primary screen. Additional validation experiments are required to confirm hits as well as elucidate the mechanisms by which these genes contribute to E6-mediated degradation of p53.

Challenges of CRISPR Cas9 Technologies

CRISPR Cas9 technologies were initially discovered in 1987, but its utilization as a defense against viral invaders was not elucidated until 2007 (Barrangou, R., 2007). Genome engineering applications of CRISPR was first demonstrated only ten years ago in 2012 when Janek et al. discovered they could exploit the system and use it for RNA-programmable genome editing (Jinek, M., 2012). CRISPR methods have come a long way in the past decade becoming more efficient and accessible, however the technology is still improving and expanding into different fields and applications.

There are several different transfection techniques compatible with CRISPR Cas9 technologies; the methods range from physical techniques such as electroporation or microinjection to viral or lipid nanoparticle-mediated delivery (Ringer, K. P., 2018). Each method of delivery poses its own challenges and drawbacks, however, having multiple options makes genome editing via CRISPR more versatile and allows researchers to choose a technique that is most compatible to their experiments (Agrotis, A., 2015). The lipid-mediated CRISPR Cas9 technique was chosen for this project because it was most conducive to high throughput format, the reagents are widely available, it takes significantly less time than viral-mediated transduction and is significantly less expensive than electroporation (Ringer, K. P., 2018). In this experiment, the cells were engineered to express Cas9 using an inducible promoter. While stable Cas9 cell lines allow for easier handling, this strategy was chosen to avoid any phenotypic artifacts or harmful consequences of continuous Cas9 expression. This method was also chosen over co-delivering the enzyme with the sgRNA because Cas9 is quite large making it difficult to

introduce into cells; it is also more cost effective to have the cells expressing Cas9 than having to purchase Cas9 mRNA or protein (Agrotis, A., 2015). The sgRNA was added to a transfection mixture containing lipofectamine transfection reagent, and the molecules were allowed to complex while the cell suspension was being prepared. Once the cells were introduced into the system, the lipid nanoparticles delivered the sgRNA into the nuclei of the cells, allowing the sgRNA to bind Cas9 and bring the enzyme to the correct target sequence in the genome to generate a knockout of the specified gene.

A successful knockout using lipofectamine-based transfection methods relies on multiple processes to occur efficiently, therefore there were several aspects that had to be carefully considered and optimized for this high throughput screen to be successfully performed. Lipofectamine is one of the most common and commercially available lipid nanoparticle delivery system, however there is still much to improve (Agrotis, A., 2015). The reagent complexes with the negatively charged nucleic acids in the sgRNA and then fuses with negatively charged cell membranes to bring the material into the cell. Once in the cell, the complex must escape the endosome to avoid being degraded by the lysosomal pathway and translocate to the nucleus (Agrotis, A., 2015). Wang et al. could achieve ~70% in vitro modification efficiency, however, the group was using custom reagents that were designed specifically for their system (Wang, M., 2016). While it was impractical to assess transfection efficiency across the screen of ~8,500 cellular targets, lower efficiencies were expected and observed compared to screens utilizing siRNA technologies. The design of sgRNAs and their DNA target site also influence the efficacy of the CRISPR Cas9 system. Single and multiple-base mismatches can be tolerated if they are further away from the PAM, however, because CRISPR uses shorter target

sequences compared to other gene editing methods it may have comparatively decreased specificity (Cradick, T. J., 2013). The sgRNA design is typically responsible for any off-target effects, and therefore the sequence should be carefully designed and cross referenced to generate efficient guides (Lino, C. A., 2018). The human arrayed CRISPR library that we used was designed by Synthego utilizing their in-house computational tools and software packages, with validation exclusively done via electroporation delivery. It is expected that some guides might not be optimally designed to work with the delivery method, cell line, and or post transfection incubation period utilized in our experiments, therefore it is important to not overinterpret any negative results.

It is imperative for the success of a high throughput CRISPR screen to have the maximum number of cells expressing Cas9 at the time of transfection, so the enzyme is available for the sgRNA to bind. We were able to consistently have > 80% of cells expressing Cas9 at the time of transfection through induction with 5.85µM doxycycline 48h in advance of transfection. By including 5.85µM doxycycline in the media at the time of transfection, Cas9 expression was maintained for at least another 48h. Although 80% is relatively high, it is important to acknowledge that the ~20% of cells not expressing Cas9 were not capable of having their genomes edited. Even among the Cas9 expressing cells, some genes will not be knocked down due to the inaccessibility of their target sequences. The large Cas9 enzyme may not be able to bind if it is blocked by cognate DNA-binding proteins or the target region has high levels of topological complexity (Wu, X., 2019). It is possible some genes may also require longer incubation periods than 96 hours to be knocked out and develop an observable phenotype. CRISPR technologies require long incubation times, typically more than three days, to allow for

genome editing to occur. Incubating cells in microplates for long periods of time poses challenges with overgrowth and subsequent high-content analysis (Agrotis, A., 2015).

Considering all the posed challenges of conducting high throughput CRISPR Cas9 experiments, the minimal values of 10% p53+ cells/ well or 15 cells that were p53+/ well are reasonable criteria for potential hits. The background levels of p53 stabilization were also very low, typically below 1% or only a couple p53+ cells per well, which also allowed the hit picking criteria to be set at relatively low values. Due to the challenging nature of this novel technology, low transfection efficiencies and phenotypic responses were expected compared to more developed methods. Researchers have utilized RNA interfering (RNAi) technologies to knockdown genes of interest for over 20 years (Mohr, S. E., 2014). In that time the reagents, design algorithms, and overall transfection efficiency has been optimized, therefore it is reasonable to expect more robust phenotypic responses with more stringent analyses for hit calling criteria.

Essential Cancer Gene Knockouts

Successful transfection of sgRNA targeting essential genes caused a drastic reduction in cell number, this demonstrates that the assay was effective at generating knockouts. There were four genes, aside from the expected KIF11 gene, that when knocked out had less than 50 cells/well remaining after 96h. This is a significant reduction from wells that were transfected with NLRP5 sgRNA that typically contained 1,500 – 2,500 cells/well. These 4 essential genes were HIST1H4C, RAN, VCP, and PLK1. One group discovered that downregulating the expression of the histone H4C gene

with small molecule or siRNA treatment in human colon cancer cells leads to the arrest of proliferation (Dickinson, L. A., 2004). In head and neck squamous cell carcinoma cells the RAN gene was shown to promote proliferation (Zhang, C., 2020), which supports why reduced proliferation was observed in cervical cancer RAN knockout cells. The Vasolin-Containing Protein VCP gene or p97 is a known prognostic biomarker and therapeutic target in cancer because of its involvement in different cellular processes that are critical for cancer cell survival and aggressiveness (Costantini, S., 2021). Knockdown of VCP in colorectal, gastric, esophageal, bone, head, neck, and other cancers led to the inhibition of cellular proliferation and induction of apoptosis (Costantini, S., 2021). PLK1 is another potential target for cancer therapy because its inhibition in cancer cells interferes with mitosis and causes cell death (Liu, Z., Sun, 2016). Taken together, it is reasonable to conclude that HIST1H4C, RAN, VCP, and PLK1 are all essential for cervical cancer cell survival as supported by the reduction in cell number observed in the assay.

Primary Screen Hits

Eight genes targeting proteasomal subunits that scored positive in the siRNA screen were reconfirmed in the CRISPR screen: PSMA6, PSMB6, PSMD1, PSMD14, PSMC1, PSMD7, PSMD2, and PSMB4. Guides targeting PSMA2 and PSMA4 were used as controls in the assay and 22 proteasomal subunits scored positive in the top 152 hits. These findings are consistent with the mechanism by which HPV E6 promotes the ubiquitin mediated proteolysis of p53 in cervical cancer cells. If a knockout of important proteasome proteins is generated, then the proteasome cannot function to degrade the

ubiquitylated p53 proteins. It is encouraging that these genes scored positive and adds confidence to other potential hits discovered in the screen.

We were surprised that only two of the non-proteasomal subunit genes, NDUFA6 and MAP3K9, reconfirmed from the siRNA screen that did not encode for a proteasomal subunit. While the siRNA and sgRNA libraries included different genes, there were only 7 hits in the CRISPR screen that were not tested in the siRNA screen. This means 135 of the sgRNA hits were not consistent with the findings of the siRNA screen. The criteria for identifying potential hits varied between the two screens, with a greater percentage of cells needing to display p53 stabilization and overall protein levels remain unaffected in the live-cell siRNA screen. RNAi technology is a powerful tool to conduct loss-of-function screening, but the method results in incomplete protein depletion and often produces miRNA-like off-target effects (Wang, F., 2018). It is possible some of the siRNA screen hits that did not reconfirm in the CRISPR screen were due to off target effects or the different phenotype observed when a protein is knocked down compared to being knocked out. It is probable that the false negatives in the CRISPR screen were a result of the challenging nature of the technology and insufficient knock out. The sgRNA design for these genes were likely not compatible as supported by the tested sgRNA targeting E6AP, which in theory should have worked to stabilize p53.

Out of the 152 genes that scored positive for p53 stabilization, there were a couple novel genes that scored very high and have literature to support their involvement in cervical cancer. The gene with the largest number of p53+ cells was Chromosomal segregation 1 like (CSE1L) with an average of 71 positive cells across the three replicates, resulting in an average of 9.8% of cells expressing p53 across the three

replicates. CSE1L encodes a protein that promotes transcriptional coactivator with PDZ-binding motif (TAZ) accumulation in the nuclei of cancer cells (Nagashima, S., 2021). TAZ is upregulated in cervical and other cancerous cells; in cervical cancer TAZ induces transcription of PD-L1 to promote proliferation, anti-apoptosis, migration, and invasion (Han, Y., 2021). TAZ is also known to negatively regulate the tumor suppressor functions of p53 and attenuate p53-mediated cellular senescence (Miyajima, C., 2020). Multiple studies have found there is a regulatory interaction between CSE1L and p53 in several tumor cell lines (Alnabulsi, A., 2012). One study found that suppressing CSE1L expression reduces proliferation, invasion, and migration and increases apoptosis in nasopharyngeal carcinoma cells (Luo, Y., 2021). Taken together with the findings of this screen, it is possible a knockout of CSE1L results in decreased TAZ in the nuclei of cervical cancer cells and results in p53 stabilization. CSE1L should be further investigated in its role of stabilizing p53 in cervical cancer cell lines.

The gene that had the highest percentage of p53+ cells was Karyopherin beta 1 (KPNB1) with an average of 37.2% across the three replicates, which was significantly higher than the positive controls, and had an average of 30 p53+ cells across the three replicates. KPNB1 is the main nuclear import protein involved in transporting materials from the cytoplasm to the nucleus (Carden, S., 2018). One study found that HPV E6 interacts with KPNB1 to enter the nuclei of host cells (Le Roux, L. G., 2003). The KPNB1 gene is significantly overexpressed in cervical cancers, and studies have shown inhibiting the gene leads to cancer cell death while non-cancerous cells were minimally affected (Carden, S., 2018). If HPV E6 cannot enter the nucleus and interact with cellular protein E6AP to ubiquitinate p53, then p53 localized in the nucleus will not be degraded.

It is important to note p53 may also be found in the cytoplasm (Green, D. R., 2009) and these proteins would still be susceptible to E6-mediated degradation. The cell line used in the assay expressed mutant R273C p53 which is less proapoptotic as WT p53, this explains why significant cancer cell death was not observed like in studies conducted by Carden et al. KPNB1 is a strong candidate for cellular genes that aid in the stabilization of p53 in HPV+ cells and should be further investigated as a potential preventative therapeutic target.

This screen was successful in overcoming the challenges of CRISPR technologies, particularly in 384-well format, to identify 152 potential cellular genes that are involved in p53 degradation in cervical cancer cells. It is our hope that the knowledge gained from developing and optimizing this assay will provide guidance for future high throughput CRISPR screens. These findings also provide more than 100 genes to be validated and further investigated for their therapeutic potential to treat HPV+ lesions.

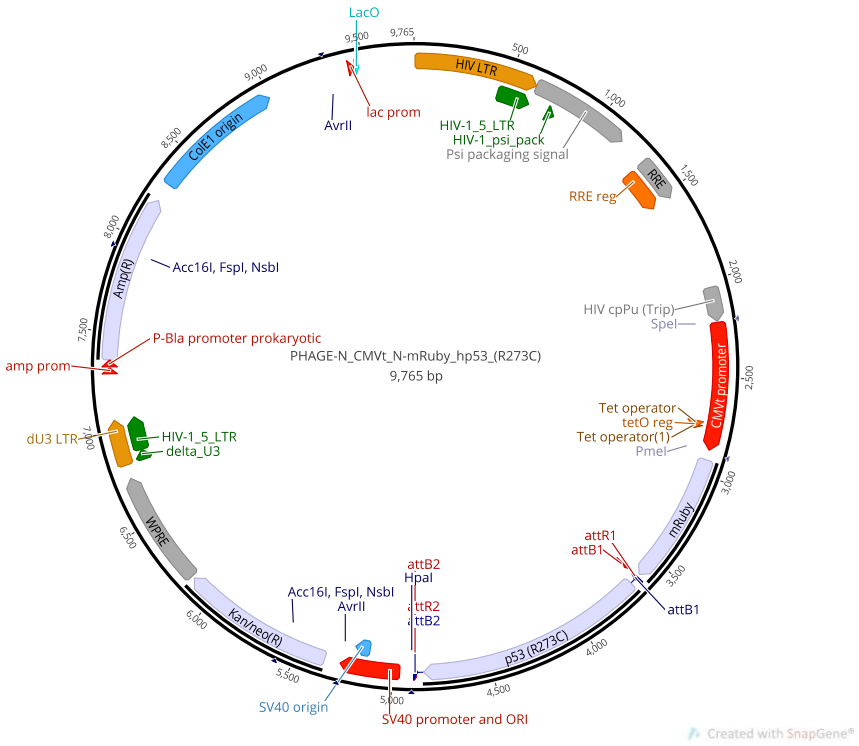

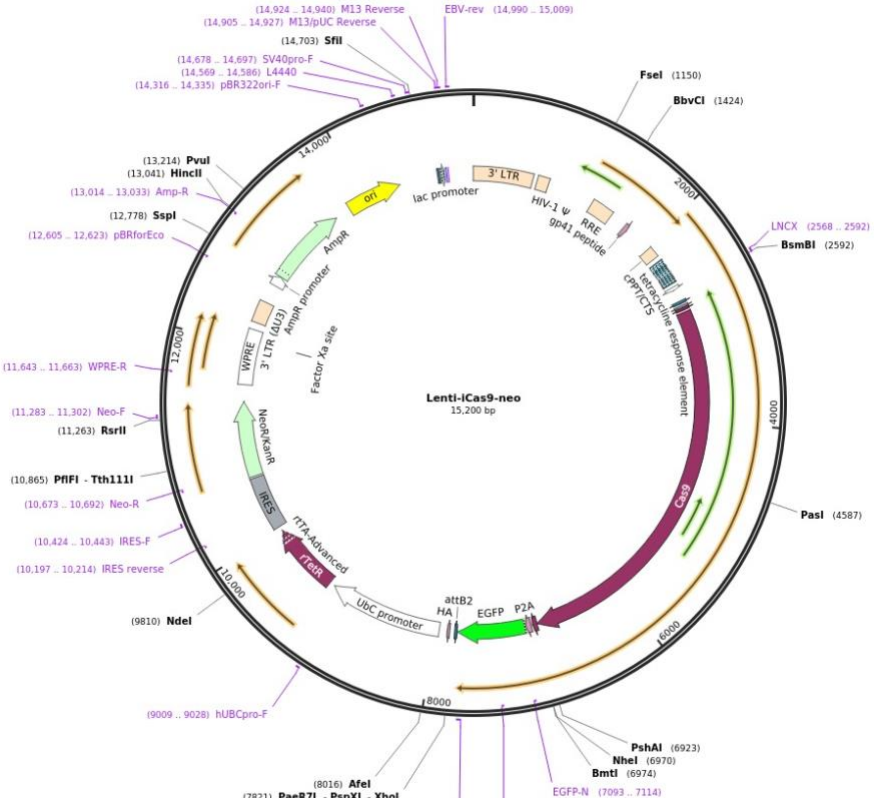

Figure 1. Plasmid Maps.

Maps of iCas9-eGFP (A) and R273C p53-mRuby (B) plasmids.

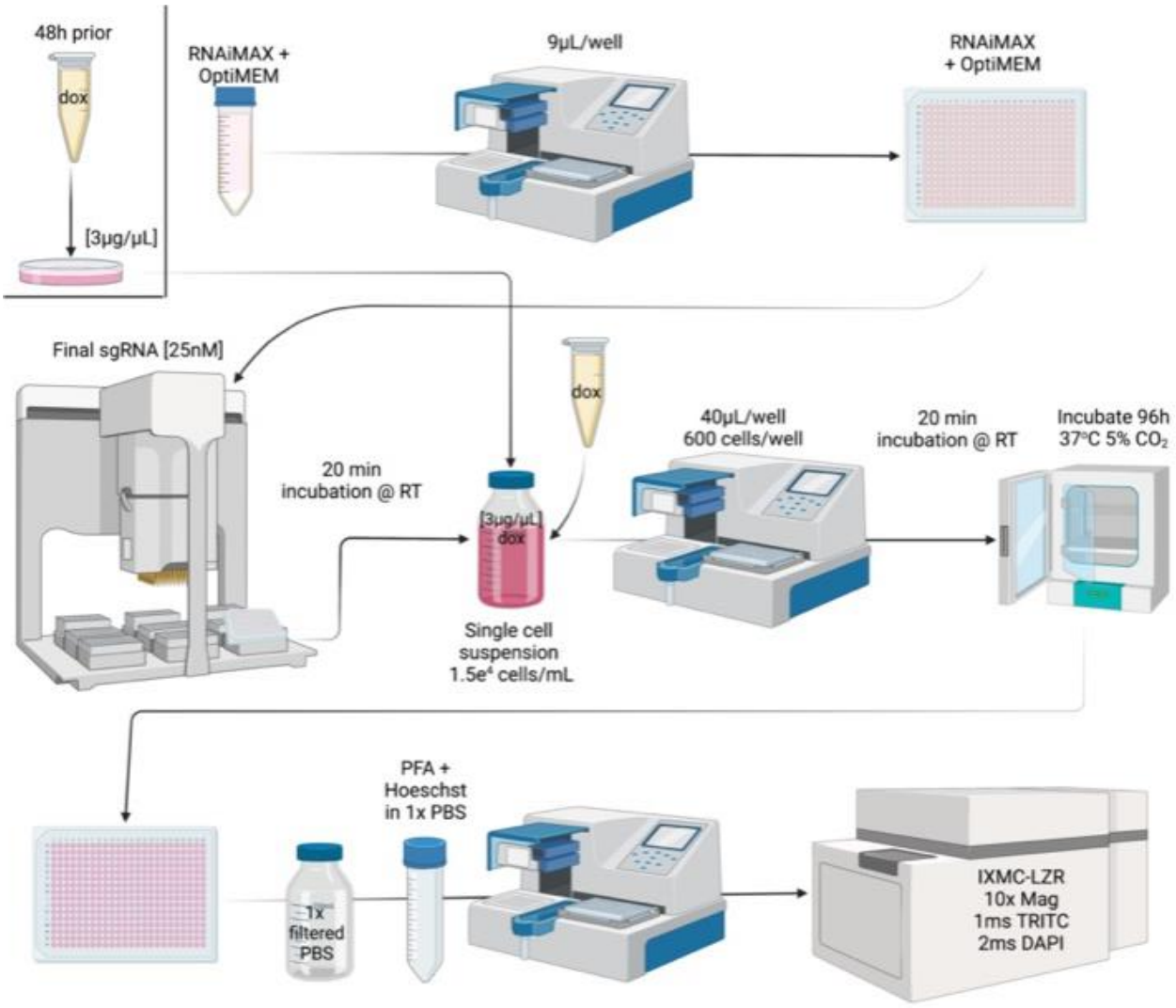

Figure 2. Workflow Diagram.

Finalized screening workflow.

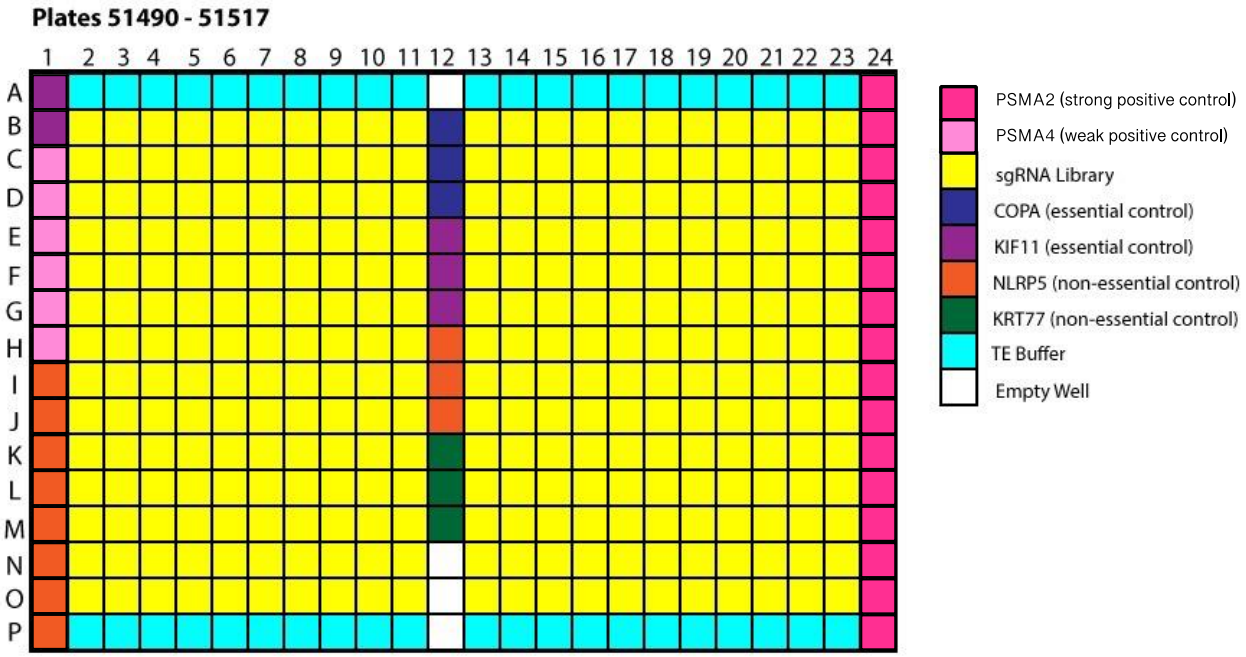

Figure 3. Library Plate Layout.

Library plate layout with pre-loaded controls in column 12. The assay-specific positive and negative controls depicted in columns 1 and 24 were added to assay plates from another 384-well microplate, taking advantage of the empty wells in the library plate.

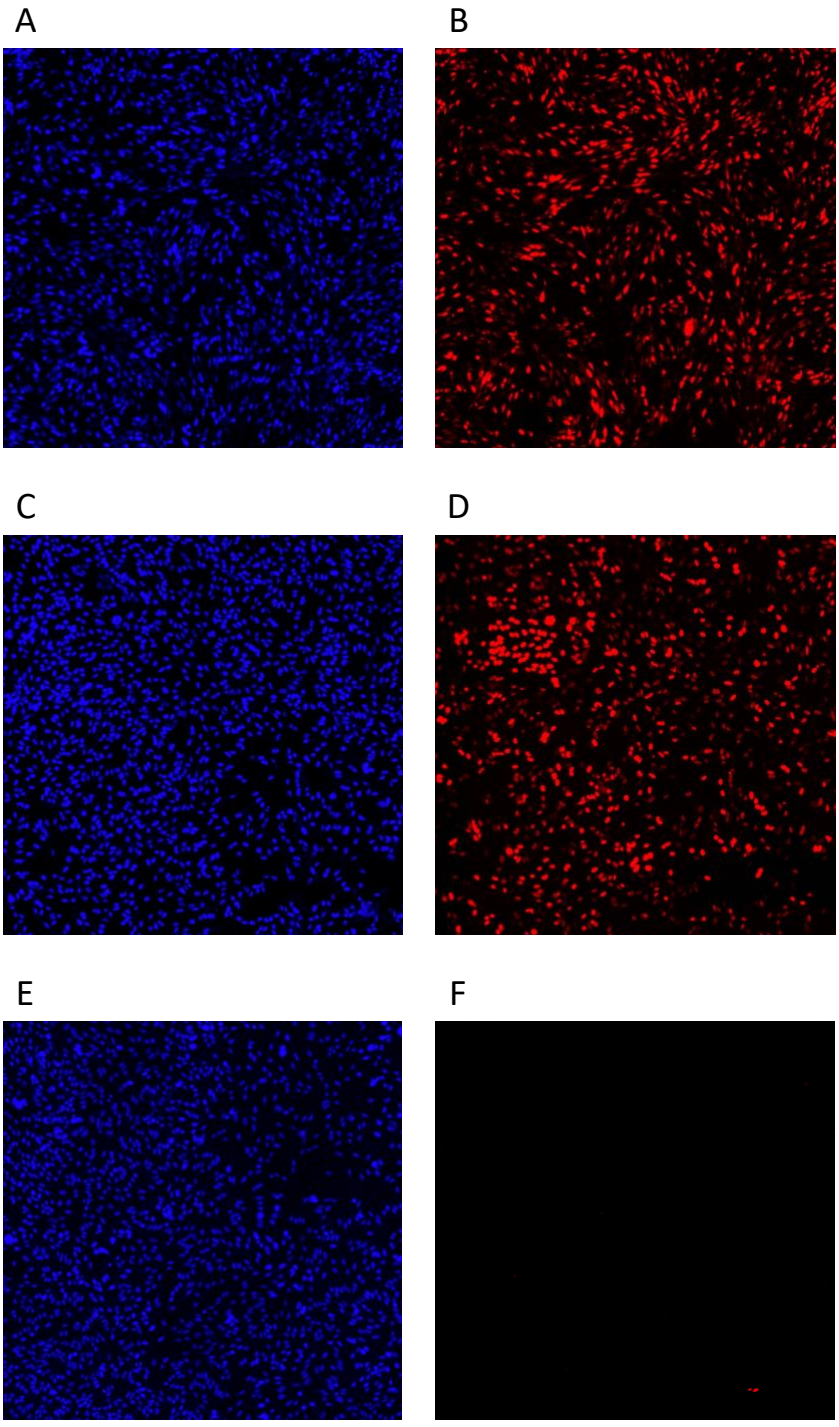

Figure 4. Compound and siRNA Induced p53 Stabilization.

A) Total nuclei and B) p53+ cells when treated with Bortezomib [500nM] 24h. C) Total nuclei and D) p53+ cells when transfected with 25nM E6AP siRNA 72h. E) Total nuclei and F) p53+ cells non-treated. Acquired with 4x magnification.

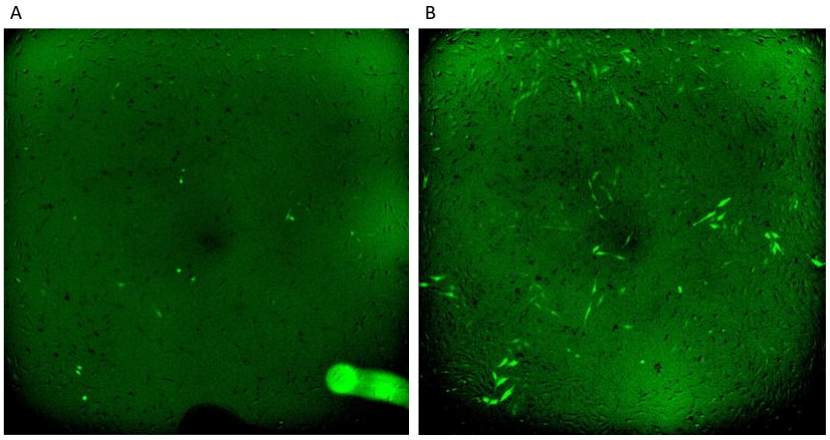

Figure 5. Cas9 Expression at 24h and 48h.

Live GFP+ cells acquired utilizing FITC wavelength at A) 24h and B) 48h post incubation with 5.85µM doxycycline on Optika's B-510FL benchtop fluorescent microscope at 10x magnification.

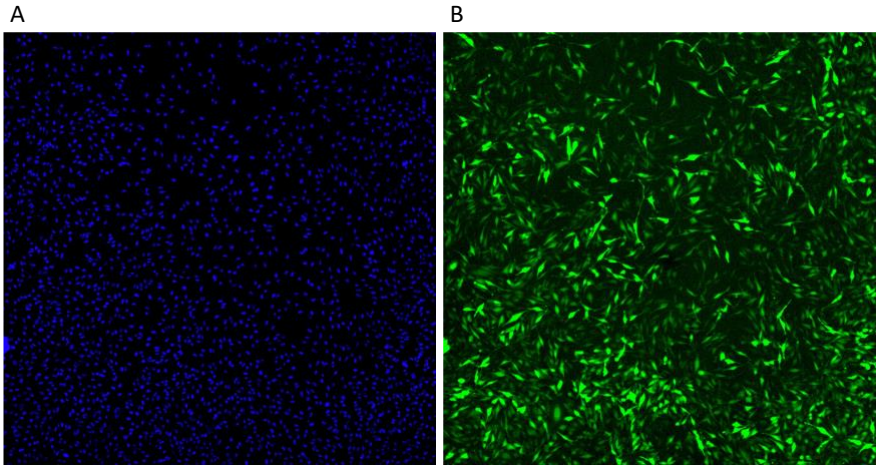

Figure 6. Cas9 Expression.

A) Nuclei and B) GFP+ cells acquired utilizing FITC wavelength on IXM-C. 48h incubation with 3µg/µL of doxycycline. Acquired with 4x magnification.

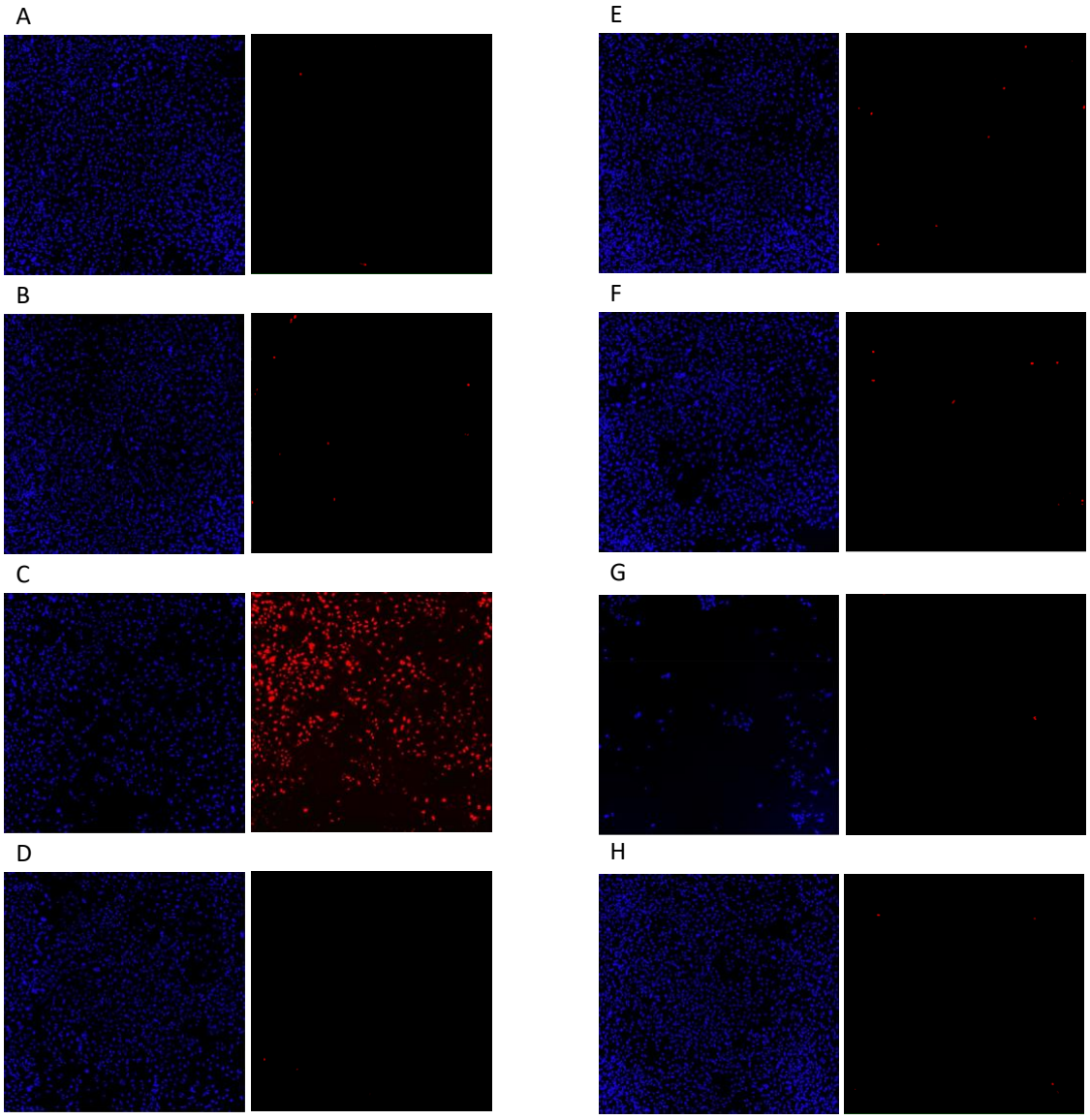

Figure 7. E6AP sgRNA.

A) pooled E6AP sgRNA B) E6AP sgRNA 3 C) E6AP siRNA D) NLRP5 sgRNA E) E6AP sgRNA 2 F) E6AP sgRNA 1 G) KIF11 sgRNA transfected at 25nM for 96h. H) non-treated cells. Acquired with 4x magnification.

Plate 51510 %p53+ heat map

	1	2	3	4	5	6	7	8	9	10	11	12	13	14	15	16	17	18	19	20	21	22	23	24
A	6.09	0.77	0.40	0.21	0.23	0.56	0.41	0.18	0.38	0.32	0.18	0.29	0.41	0.25	0.19	0.34	0.34	0.26	0.46	0.30	0.68	0.57	0.99	3.73
B	7.99	9.33	0.30	12.24	3.50	4.55	4.78	3.12	0.51	0.08	17.68	11.65	0.42	25.38	2.40	0.95	2.26	26.68	5.72	5.32	17.04	0.80	5.03	1.94
C	5.23	4.56	4.55	1.13	1.31	0.70	7.47	16.47	1.86	0.51	0.24	4.85	4.04	0.11	3.30	8.96	0.52	8.17	34.98	0.25	9.20	4.13	18.89	2.89
D	8.00	0.78	0.42	0.31	0.91	0.58	1.06	19.18	1.00	0.39	0.43	6.80	4.31	1.31	22.48	2.74	2.22	27.91	25.01	1.79	0.82	2.57	16.28	1.86
E	11.56	0.26	0.35	0.17	0.82	4.29	3.91	0.71	0.25	0.49	0.33	5.10	1.95	1.06	12.83	0.20	6.93	0.85	23.43	0.52	0.57	26.88	2.90	1.72
F	12.75	0.25	22.86	0.33	4.65	1.57	0.23	5.26	0.37	11.68	0.30	3.74	5.54	29.29	0.19	6.91	0.15	0.31	30.58	0.61	0.27	0.94	14.86	1.42
G	3.78	1.05	2.19	0.24	0.31	1.28	7.94	0.22	0.38	1.28	1.31	6.21	1.06	0.48	0.17	1.21	1.02	31.26	17.10	0.24	0.60	10.59	2.27	1.88
H	7.43	19.77	0.13	32.26	0.30	0.24	13.20	23.22	0.18	0.96	0.16	0.45	0.76	0.36	0.58	0.22	2.98	19.49	2.17	2.38	1.69	0.67	0.67	2.49
I	2.97	2.97	0.69	2.25	8.46	9.67	4.21	1.27	0.59	0.17	2.49	0.56	0.96	0.26	1.02	0.63	0.44	8.06	9.90	0.15	4.77	3.38	25.94	5.44
J	2.41	21.31	14.83	0.28	0.09	13.26	0.12	0.31	4.80	0.08	0.21	0.22	0.05	0.19	0.05	0.29	26.57	20.49	24.45	0.21	0.17	0.78	19.14	5.22
K	2.56	0.41	27.57	0.07	2.39	0.03	0.17	0.20	0.61	0.40	3.42	0.28	1.15	0.08	0.85	0.66	37.22	18.36	4.95	9.24	0.78	3.16	1.46	6.91
L	3.85	1.16	26.34	14.05	0.23	0.29	0.26	0.18	4.57	0.47	0.09	0.46	0.68	0.26	0.10	0.89	26.66	32.34	9.61	4.79	0.23	32.25	12.56	7.86
M	2.72	0.50	0.74	10.21	5.67	0.31	0.07	1.05	0.47	0.12	0.62	0.62	0.31	0.31	1.11	0.42	18.39	0.34	13.70	0.26	3.87	0.22	11.46	8.71
N	3.12	27.66	0.22	8.67	0.47	0.14	4.03	0.08	0.27	0.38	0.10	0.47	0.41	5.88	0.27	0.20	28.35	13.21	0.57	0.79	1.56	0.71	0.25	7.70
O	4.00	0.75	0.38	0.45	0.14	1.01	1.46	1.19	0.31	0.35	1.04	0.16	0.26	0.29	0.59	0.09	25.02	29.80	0.49	0.19	0.17	0.30	0.22	3.76
P	4.49	0.31	0.18	0.18	0.28	0.26	0.18	0.10	0.13	0.15	0.27	0.14	0.87	0.11	0.49	0.28	0.17	0.24	0.11	0.17	0.25	0.20	0.40	3.22

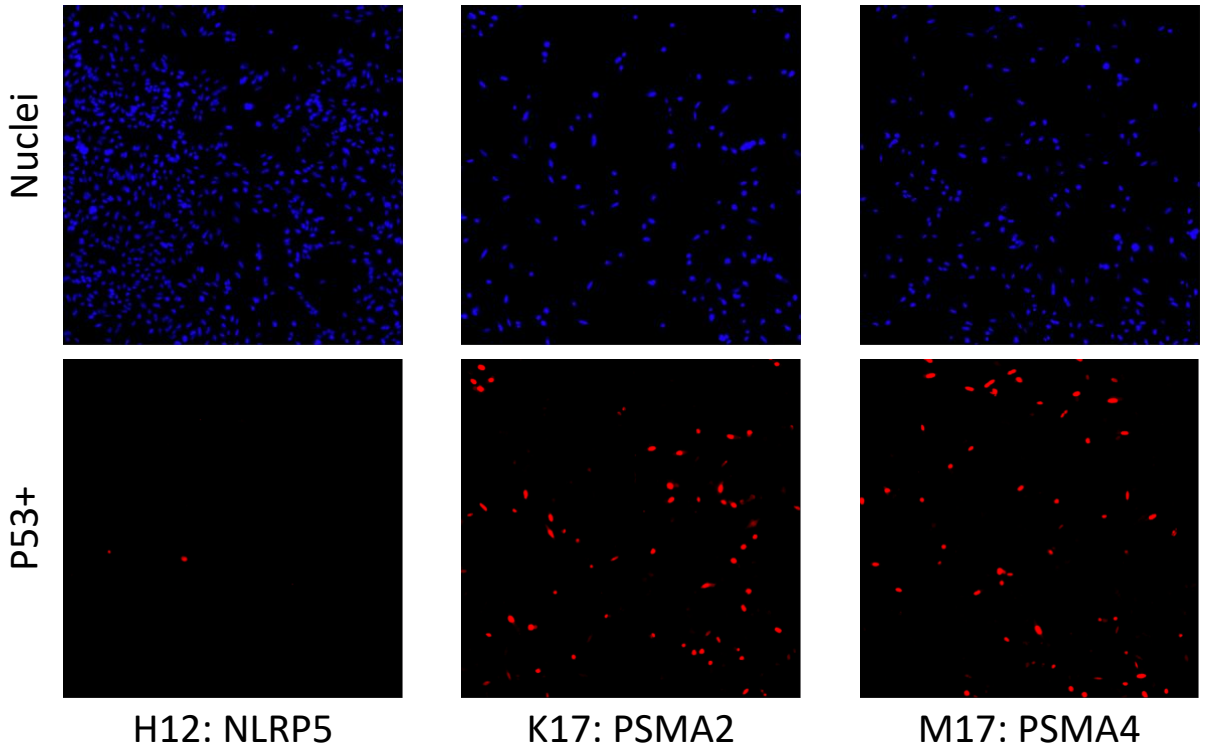

Figure 8. Library Plate 51510.

Heat map of plate #51510 and corresponding images of nuclei and p53+ cells for wells treated with sgRNA targeting NLRP5 (H12), PSMA2 (K17) and PSMA4 (M17). Additional controls were placed wells A1-H1 (KIF11), I1-P1 (NLRP5), A24-H24 (E6AP pool of 3 sgRNA), and I24-P24 (E6AP #3) Images were acquired 96h post-transfection on the IXM-C using 10x magnification.

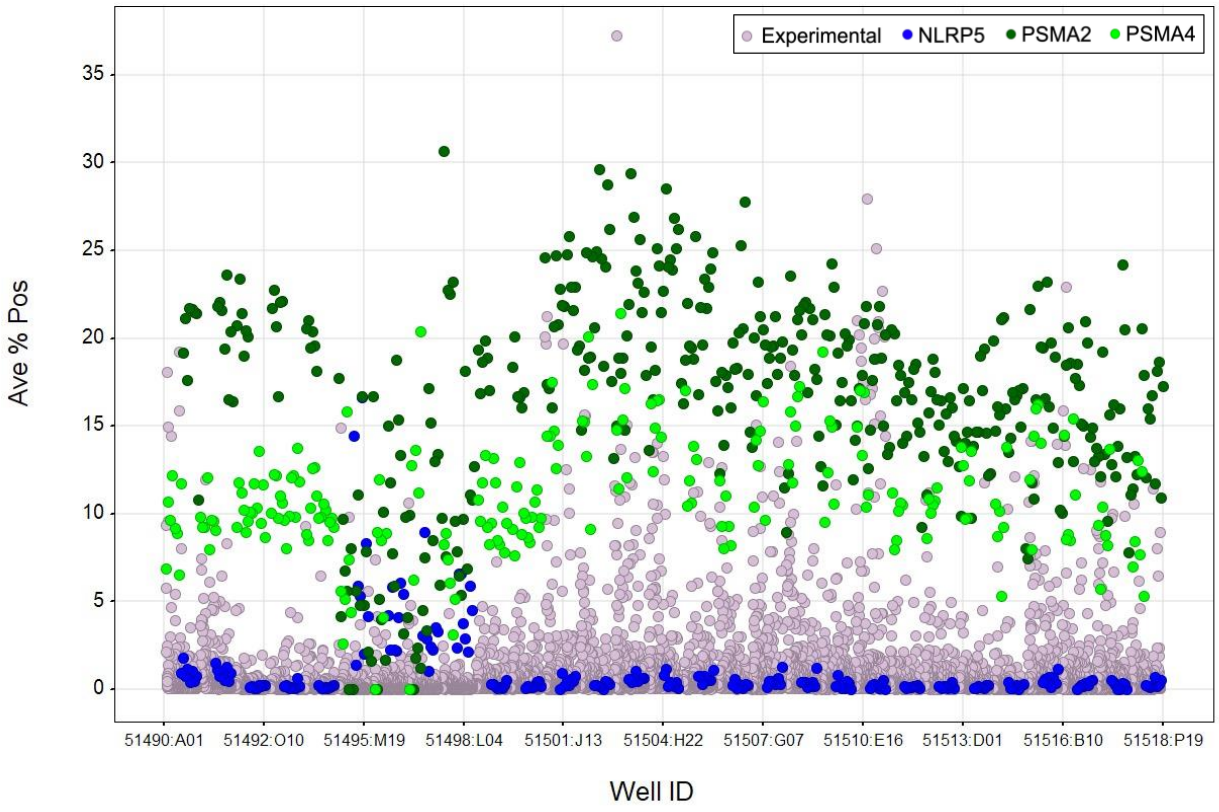

Figure 9. Comparing Positive Controls.

Scatter plot with the average % p53+ cells on the Y-axis and Well ID (library plate number and well) on the X-axis. Experimental wells are indicated by the gray circles, while negative control sgRNA is represented by the blue circles and positive control sgRNAs are shown in green

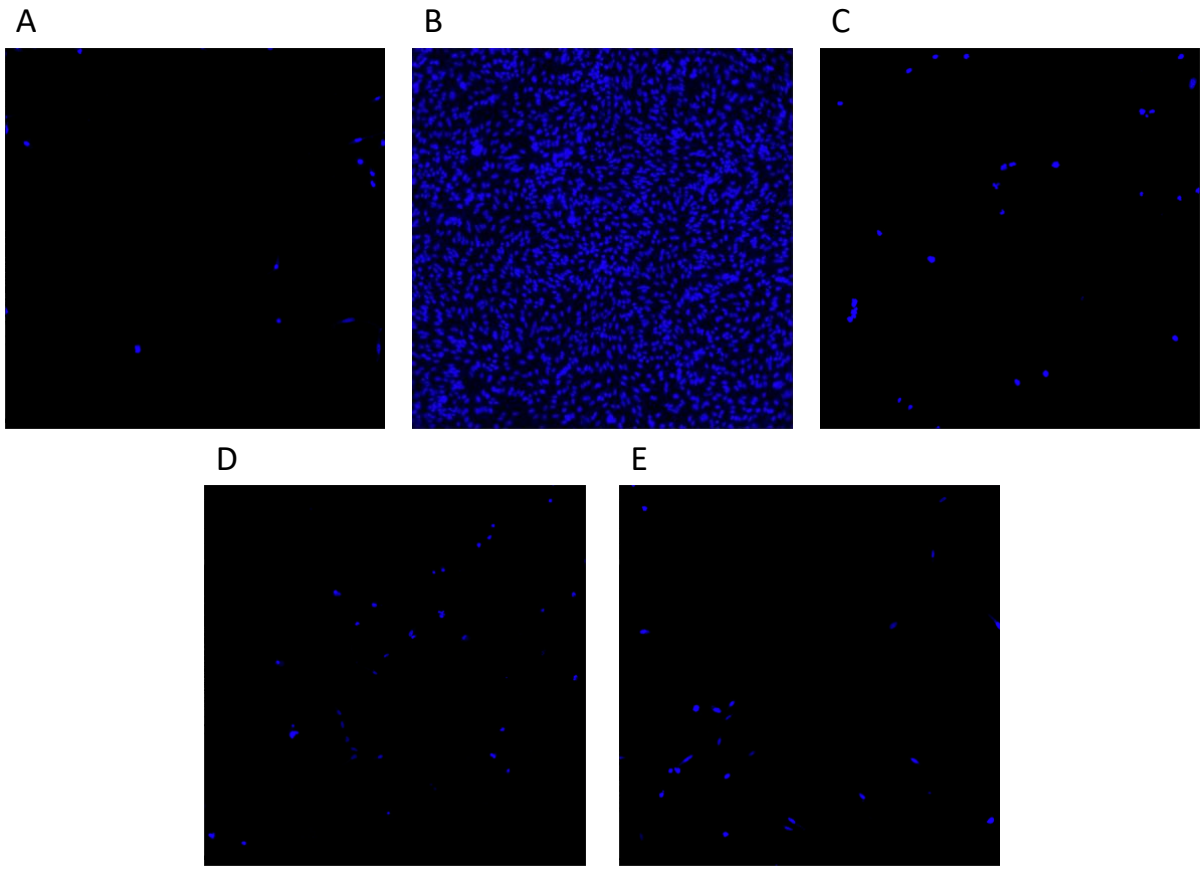

Figure 10. Cell Death Inducing Hits.

Images acquired in the DAPI channel of Hoechst-stained nuclei in wells transfected with sgRNA targeting A) HIST1H4C, B) NLRP5, C) PLK1, D) RAN, and E) VCP.

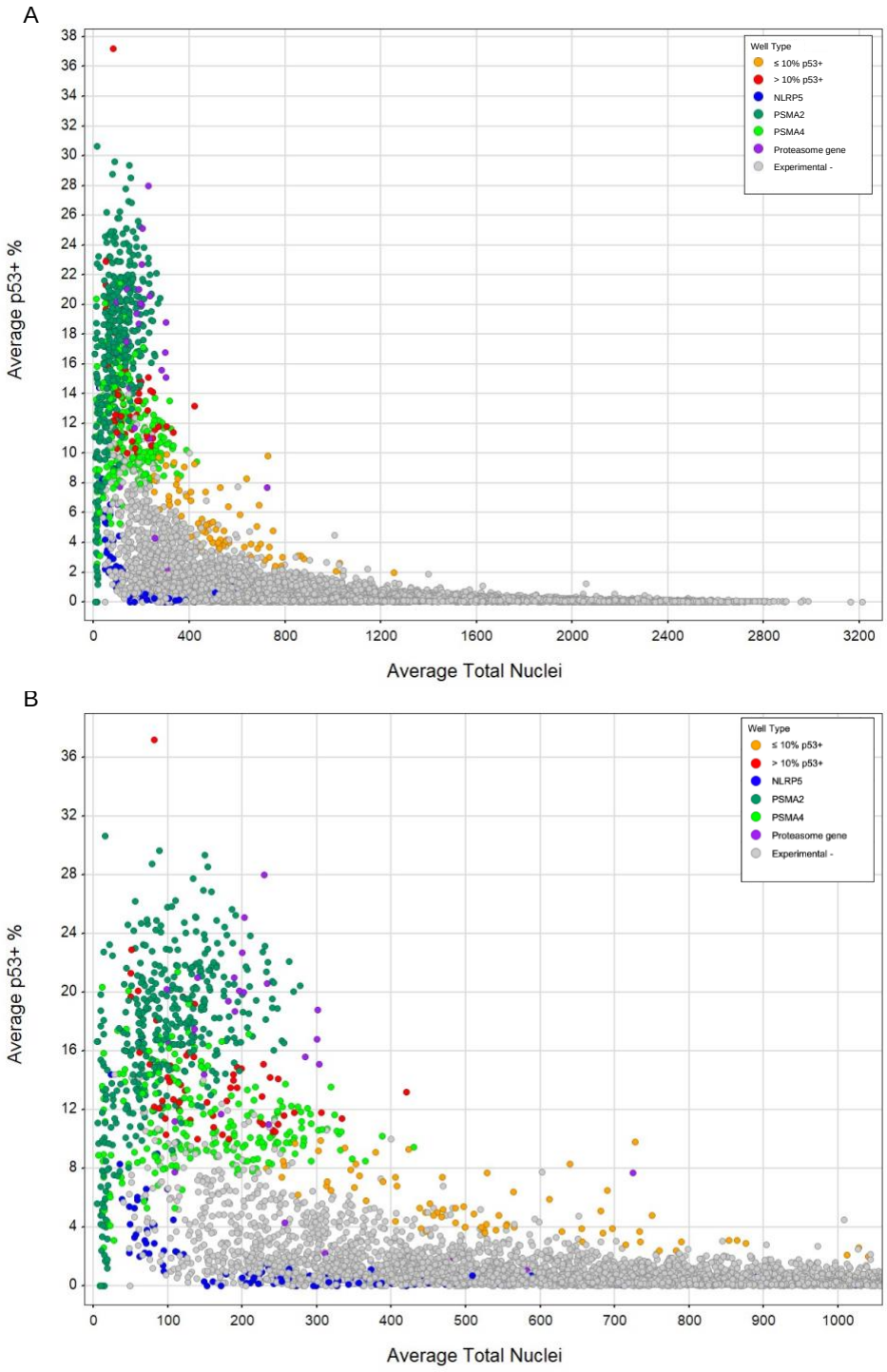

Figure 11. Percent p53+ Versus Cell Count.

Average total nuclei across the three replicates on the X-axis and average %p53+ across three replicates plotted on the Y-axis. Full library data set plotted in A) and B) the same graph looking closer at nuclei counts < 1000 cells.

Table 1. Top Death Inducing Hits.

Entrezgene Symbol	Entrezgene ID	Total Nuclei
HIST1H4C	8364	28
KIF11	3832	40
RAN	5901	48
VCP	7415	48
PLK1	5347	49
IL18R1	8809	50
HNRNPK	3190	50
TRAPPC6B	122553	51
TDP1	55775	51
SRSF1	6426	51
SPOCK1	6695	51
TEC	7006	54
HK1	3098	60
USP30	84749	60
HSPA5	3309	60
STC2	8614	61
TMEM59	9528	61
PCDHGC3	5098	63
TUBA1B	10376	66
TAPBPL	55080	67
TRIM10	10107	67
TRIM35	23087	69
ZNF511-PRAP1	104326056	70
VCL	7414	70
TBC1D4	9882	72
TUBB	203068	73
HNRNPL	3191	73
UQCRC2	7385	73
OR5B17	219965	75
ZDHHC20	253832	75
TUFT1	7286	79
USP21	27005	79
HNRNPM	4670	80
TAS2R30	259293	81
KPNB1	3837	82
TSPEAR	54084	82
ZDHHC15	158866	83
ACRBP	84519	84
TAP1	6890	86
SNU13	4809	89
IKBKG	8517	89
SOSTDC1	25928	90
USP42	84132	90
SSTR1	6751	91
TECTA	7007	91
USP7	7874	92
TNNI3	7137	92
USP51	158880	97
PRRG2	5639	97
ZPLD1	131368	97
PSMC5	5705	98
STEAP1	26872	99

52 genes with < 100 cells remaining on average across the three replicates.

Table 2. Top 152 Hits.

Entrezgene ID	Entrezgene Symbol	Flag Low Cell	Avg Pos Red Count	Average % p53+	siRNA Screen +
3837	KPNB1	Y	30	37.2	no
5690	PSMB2		63	28.0	no
5683	PSMA2		51	25.1	no
122553	TRAPPC6B	Y	11	22.9	no
5686	PSMA5		47	22.7	no
8809	IL18R1	Y	10	21.3	no
5688	PSMA7		30	21.0	no
5684	PSMA3		39	21.0	no
5695	PSMB7		48	20.6	no
5705	PSMC5	Y	20	20.2	no
3098	HK1	Y	14	20.1	no
5687	PSMA6		38	20.1	yes
5682	PSMA1		39	20.0	no
3190	HNRNPK	Y	10	19.7	no
3241	HPCAL1	Y	23	19.7	no
5706	PSMC6		33	19.4	no
51166	AADAT	Y	26	19.2	no
5694	PSMB6		57	18.8	yes
5689	PSMB1		35	18.7	no
5098	PCDHGC3	Y	12	18.4	no
84519	ACRBP	Y	15	18.1	no
5707	PSMD1		23	17.5	yes
10213	PSMD14		23	17.1	yes
5691	PSMB3		50	16.8	no
5717	PSMD11	Y	17	16.5	no
22	ABCB7		20	15.9	no
9528	TMEM59	Y	10	15.9	no
54973	INTS11	Y	20	15.7	no
5685	PSMA4		44	15.6	no
3750	KCND1	Y	20	15.6	no
5693	PSMB5		45	15.1	no
84634	KISS1R		31	15.1	no
219965	OR5B17	Y	11	15.1	no
132	ADK	Y	15	15.0	no
1447	CSN2		28	14.9	no
1902	LPAR1		28	14.8	no
19	ABCA1		27	14.4	no

Entrezgene ID	Entrezgene Symbol	Flag Low Cell	Avg Pos Red Count	Average % p53+	siRNA Screen +
5700	PSMC1		21	14.4	yes
26872	STEAP1	Y	13	14.2	no
27250	PDCD4		34	14.2	no
127066	OR14C36		35	14.1	not tested
4236	MFAP1		26	14.0	no
23731	TMEM245	Y	14	13.9	no
3998	LMAN1	Y	16	13.7	no
57633	LRRN1		24	13.5	no
2847	MCHR1		23	13.5	no
55793	MINDY1		16	13.3	no
653499	LGALS7B		53	13.2	not tested
4700	NDUFA6		30	12.9	yes
402135	OR5K2	Y	14	12.7	no
10204	NUTF2		23	12.6	no
7137	TNNI3	Y	11	12.6	no
84818	IL17RC		21	12.5	no
343641	TGM6	Y	15	12.5	no
259293	TAS2R30	Y	10	12.2	not tested
4809	SNU13	Y	11	12.1	no
84883	AIFM2	Y	16	12.0	no
3815	KIT		29	11.8	no
23450	SF3B3		29	11.8	no
5713	PSMD7		20	11.7	yes
151230	KLHL23		29	11.6	no
8689	KRT36		15	11.6	no
158880	USP51	Y	11	11.4	no
3183	HNRNPC		39	11.4	no
4017	LOXL2		15	11.3	no
6167	RPL37		25	11.2	no
338674	OR5F1		26	11.0	no
5708	PSMD2		26	11.0	yes
441670	OR4M1		25	11.0	no
6303	SAT1		17	10.8	no
9343	EFTUD2		25	10.6	no
4074	M6PR		25	10.5	no
54674	LRRN3		24	10.5	no
6634	SNRPD3		18	10.3	no
5639	PRRG2	Y	10	10.3	no
5024	P2RX3		18	10.0	no

Entrezgene ID	Entrezgene Symbol	Flag Low Cell	Avg Pos Red Count	Average % p53+	siRNA Screen +
7334	UBE2N	Y	13	10.0	no
4539	MT-ND4L		30	9.9	no
1434	CSE1L		71	9.8	no
10234	LRRC17		26	9.7	no
259249	MRGPRX1		31	9.4	no
10397	NDRG1		38	9.3	no
10746	MAP3K2		26	9.2	no
64410	KLHL25		34	9.1	no
59277	NTN4		21	8.5	no
84335	AKT1S1		18	8.3	no
9388	LIPG		27	8.3	no
3991	LIPE		21	8.2	no
55109	AGGF1		19	8.0	no
4992	OR1F1		28	7.9	no
5692	PSMB4		54	7.7	yes
54813	KLHL28		40	7.7	no
11343	MGLL		27	7.5	no
3913	LAMB2		30	7.4	no
1543	CYP1A1		32	7.4	no
390151	OR8H2		19	7.4	not tested
3850	KRT3		21	7.1	no
100528032	KLRC4-KLRK1		22	7.1	not tested
84975	MFSD5		28	6.8	no
3852	KRT5		21	6.8	no
8392	OR3A3		23	6.7	no
137797	LYPD2		20	6.5	no
468	ATF4		20	6.5	no
645745	MT1HL1		37	6.4	not tested
158038	LINGO2		17	6.2	no
55295	KLHL26		31	5.9	no
4052	LTBP1		22	5.8	no
1476	CSTB		24	5.6	no
55586	MIOX		25	5.4	no
338323	NLRP14		23	5.3	no
89782	LMLN		23	5.3	no
5106	PCK2		24	5.2	no
4147	MATN2		35	5.1	no
4772	NFATC1		22	5.0	no
51314	NME8		23	5.0	no

Entrezgene ID	Entrezgene Symbol	Flag Low Cell	Avg Pos Red Count	Average % p53+	siRNA Screen +
10461	MERTK		23	4.9	no
3866	KRT15		34	4.8	no
10876	EDDM3A		26	4.8	no
22978	NT5C2		21	4.8	no
4698	NDUFA5		22	4.7	no
8431	NR0B2		18	4.4	no
51701	NLK		21	4.3	no
27122	DKK3		23	4.2	no
53904	MYO3A		21	4.2	no
5607	MAP2K5		22	4.1	no
391191	OR2AK2		21	4.0	no
4832	NME3		20	4.0	no
8655	DYNLL1		19	4.0	no
688	KLF5		21	4.0	no
22880	MORC2		27	3.9	no
8446	DUSP11		25	3.9	no
83700	JAM3		16	3.9	no
10913	EDAR		21	3.8	no
114548	NLRP3		19	3.8	no
25973	PARS2		17	3.7	no
10047	CST8		22	3.7	no
390077	OR52N2		27	3.7	not tested
5286	PIK3C2A		18	3.6	no
131377	KLHL40		24	3.6	no
115817	DHRS1		26	3.1	no
4540	MT-ND5		26	3.1	no
116512	MRGPRD		22	3.0	no
4293	MAP3K9		20	3.0	yes
2831	NPBWR1		24	3.0	no
397	ARHGDIB		16	2.9	no
8685	MARCO		20	2.8	no
1843	DUSP1		26	2.6	no
55975	KLHL7		19	2.4	no
4842	NOS1		18	2.4	no
59084	ENPP5		22	2.1	no
1305	COL13A1		20	2.0	no
121391	KRT74		24	2.0	no

Flag Low Cell = Y if < 100 cells remaining on average across the 3 replicates.

References

Agrotis, A., & Ketteler, R. (2015). A new age in functional genomics using CRISPR/Cas9 in arrayed library screening. Frontiers in genetics, 6, 300-300. doi:10.3389/fgene.2015.00300

Alnabulsi, A., Agouni, A., Mitra, S., Garcia-Murillas, I., Carpenter, B., Bird, S., & Murray, G. I. (2012). Cellular apoptosis susceptibility (chromosome segregation 1-like, CSE1L) gene is a key regulator of apoptosis, migration and invasion in colorectal cancer. The Journal of pathology, 228(4), 471-481. doi:10.1002/path.4031

Barrangou, R., Fremaux, C., Deveau, H., Richards, M., Boyaval, P., Moineau, S., . . . Horvath, P. (2007). CRISPR provides acquired resistance against viruses in prokaryotes. Science, 315(5819), 1709-1712. doi:10.1126/science.1138140

Cao, J., Wu, L., Zhang, S. M., Lu, M., Cheung, W. K., Cai, W., . . . Yan, Q. (2016). An easy and efficient inducible CRISPR/Cas9 platform with improved specificity for multiple gene targeting. Nucleic Acids Res, 44(19), e149. doi:10.1093/nar/gkw660

Carden, S., van der Watt, P., Chi, A., Ajayi-Smith, A., Hadley, K., & Leaner, V. D. (2018). A tight balance of Karyopherin β1 expression is required in cervical cancer cells. BMC Cancer, 18(1), 1123. doi:10.1186/s12885-018-5044-8

Costantini, S., Capone, F., Polo, A., Bagnara, P., & Budillon, A. (2021). Valosin-Containing Protein (VCP)/p97: A Prognostic Biomarker and Therapeutic Target in Cancer. International journal of molecular sciences, 22(18), 10177. doi:10.3390/ijms221810177

Cradick, T. J., Fine, E. J., Antico, C. J., & Bao, G. (2013). CRISPR/Cas9 systems targeting β-globin and CCR5 genes have substantial off-target activity. Nucleic Acids Res, 41(20), 9584-9592. doi:10.1093/nar/gkt714

CRISPR History and Development for Genome Engineering. Retrieved from https://www.addgene.org/crispr/history/#:~:text=CRISPR%20(Clustered%20Regularly%20Interspaced%20Short,was%20not%20elucidated%20until%202007.

de Martel, C., Georges, D., Bray, F., Ferlay, J., & Clifford, G. M. (2020). Global burden of cancer attributable to infections in 2018: a worldwide incidence analysis. The Lancet Global Health, 8(2), e180-e190. doi:10.1016/S2214-109X(19)30488-7

de Martel, C., Plummer, M., Vignat, J., & Franceschi, S. (2017). Worldwide burden of cancer attributable to HPV by site, country and HPV type. Int J Cancer, 141(4), 664-670. doi:10.1002/ijc.30716

Dickinson, L. A., Burnett, R., Melander, C., Edelson, B. S., Arora, P. S., Dervan, P. B., & Gottesfeld, J. M. (2004). Arresting Cancer Proliferation by Small-Molecule Gene Regulation. Chemistry & biology, 11(11), 1583-1594. doi:10.1016/j.chembiol.2004.09.004

Dowhanick, J. J., McBride, A. A., & Howley, P. M. (1995). Suppression of cellular proliferation by the papillomavirus E2 protein. Journal of Virology, 69(12), 7791. Retrieved from http://jvi.asm.org/content/69/12/7791.abstract

Fields, B. N., Knipe, D. M., & Howley, P. M. (2013). Fields virology. In Fields Virology (6 ed.). Philadelphia: Wolters Kluwer Health/Lippincott Williams & Wilkins.

Francis, D. A., Schmid, S. I., & Howley, P. M. (2000). Repression of the integrated papillomavirus E6/E7 promoter is required for growth suppression of cervical cancer cells. J Virol, 74(6), 2679-2686. doi:10.1128/jvi.74.6.2679-2686.2000

Full Stack Genome Engineering. Retrieved from https://www.synthego.com/products/crispr-kits/gene-knockout-kit

Green, D. R., & Kroemer, G. (2009). Cytoplasmic functions of the tumour suppressor p53. Nature, 458(7242), 1127-1130. doi:10.1038/nature07986

Han, Y., Liu, D., & Li, L. (2021). Increased expression of TAZ and associated upregulation of PD-L1 in cervical cancer. Cancer cell international, 21(1), 592. doi:10.1186/s12935-021-02287-y

Harper, D. M., & DeMars, L. R. (2017). HPV vaccines – A review of the first decade. Gynecologic oncology, 146(1), 196-204. doi:10.1016/j.ygyno.2017.04.004

Howley, P. (2021). Fields Virology : Emerging Viruses (7

HPV and Cancer. (2021). Retrieved from https://www.cancer.gov/about-cancer/causes-prevention/risk/infectious-agents/hpv-and-cancer#:~:text=HPV%20infects%20the%20squamous%20cells,cervix%20and%20are%20called%20adenocarcinomas.

HPV Infection. July 23 2021. Retrieved from https://www.cdc.gov/hpv/parents/about-hpv.html

https://www.ncbi.nlm.nih.gov/pmc/articles/PMC1994798/

https://www.ncbi.nlm.nih.gov/pmc/articles/PMC6962986/

Human. Retrieved from https://www.gencodegenes.org/human/release_26.html

Jiang, F., & Doudna, J. A. (2017). CRISPR-Cas9 Structures and Mechanisms. Annual review of biophysics, 46(1), 505-529. doi:10.1146/annurev-biophys-062215-010822

Jinek, M., Chylinski, K., Fonfara, I., Hauer, M., Doudna, J. A., & Charpentier, E. (2012). A programmable dual-RNA-guided DNA endonuclease in adaptive bacterial immunity. Science, 337(6096), 816-821. doi:10.1126/science.1225829

Jinek, M., East, A., Cheng, A., Lin, S., Ma, E., & Doudna, J. (2013). RNA-programmed genome editing in human cells. eLife, 2, e00471. doi:10.7554/eLife.00471

Kalu, N. N., Mazumdar, T., Peng, S., Tong, P., Shen, L., Wang, J., . . . Johnson, F. M. (2018). Comprehensive pharmacogenomic profiling of human papillomavirus-positive and -negative squamous cell carcinoma identifies sensitivity to aurora kinase inhibition in KMT2D mutants. Cancer letters, 431, 64-72. doi:10.1016/j.canlet.2018.05.029

Kalu, N. N., Mazumdar, T., Tong, P., Shen, L., Wang, J., Byers, L. A., & Johnson, F. M. (2016). Abstract 3793: Cell-based, high-throughput screen for small molecule inducers of cell death in HPV-associated head and neck cancers. Cancer research (Chicago, Ill.), 76(14 Supplement), 3793-3793. doi:10.1158/1538-7445.AM2016-3793

Kelley, M. L., Keiger, K. E., Chan Jae, L. E. E., & Huibregtse, J. M. (2005). The Global Transcriptional Effects of the Human Papillomavirus E6 Protein in Cervical Carcinoma Cell Lines Are Mediated by the E6AP Ubiquitin Ligase. Journal of Virology, 79(6), 3737-3747. doi:10.1128/JVI.79.6.3737-3747.2005

Le Roux, L. G., & Moroianu, J. (2003). Nuclear entry of high-risk human papillomavirus type 16 E6 oncoprotein occurs via several pathways. Journal of Virology, 77(4), 2330-2337. doi:10.1128/jvi.77.4.2330-2337.2003

Lino, C. A., Harper, J. C., Carney, J. P., & Timlin, J. A. (2018). Delivering CRISPR: a review of the challenges and approaches. Drug delivery, 25(1), 1234-1257. doi:10.1080/10717544.2018.1474964

Liu, Z., Sun, Q., & Wang, X. (2016). PLK1 , A Potential Target for Cancer Therapy. Translational oncology, 10(1), 22-32. doi:10.1016/j.tranon.2016.10.003

Luo, Y., Qu, X., Kan, D., & Cai, B. (2021). The microRNA-451a/chromosome segregation 1-like axis suppresses cell proliferation, migration, and invasion and induces apoptosis in nasopharyngeal carcinoma. Bioengineered, 12(1), 6967-6980. doi:10.1080/21655979.2021.1975018

Martens-de Kemp, S. R., Nagel, R., Stigter-van Walsum, M., van der Meulen, I. H., van Beusechem, V. W., Braakhuis, B. J. M., & Brakenhoff, R. H. (2013). Functional Genetic Screens Identify Genes Essential for Tumor Cell Survival in Head and Neck and Lung Cancer. Clinical Cancer Research, 19(8), 1994-2003. doi:10.1158/1078-0432.Ccr-12-2539

Martínez-Noël, G., Szajner, P., Smith, J. A., Boyland, K., Kramer, R. E., & Howley, P. M. (2020). Stabilization of p53 by microRNAs in HPV-positive cervical cancer cells. bioRxiv, 2020.2009.2021.305946. doi:10.1101/2020.09.21.305946

Martínez-Noël, G., Vieira, V. C., Szajner, P., Lilienthal, E. M., Kramer, R. E., Boyland, K. A., . . . Howley, P. M. (2021). Live cell, image-based high-throughput screen to quantitate p53 stabilization and viability in human papillomavirus positive cancer cells. Virology (New York, N.Y.), 560, 96-109. doi:10.1016/j.virol.2021.05.006

Miyajima, C., Kawarada, Y., Inoue, Y., Suzuki, C., Mitamura, K., Morishita, D., . . . Hayashi, H. (2020). Transcriptional Coactivator TAZ Negatively Regulates Tumor Suppressor p53 Activity and Cellular Senescence. Cells, 9(1), 171. doi:10.3390/cells9010171

Mohr, S. E., Smith, J. A., Shamu, C. E., Neumüller, R. A., & Perrimon, N. (2014). RNAi screening comes of age: improved techniques and complementary approaches. Nature reviews. Molecular cell biology, 15(9), 591-600. doi:10.1038/nrm3860

Nagashima, S., Maruyama, J., Honda, K., Kondoh, Y., Osada, H., Nawa, M., . . . Hata, Y. (2021). CSE1L promotes nuclear accumulation of transcriptional coactivator TAZ and enhances invasiveness of human cancer cells. J Biol Chem, 297(1), 100803. doi:10.1016/j.jbc.2021.100803

Nidhi, S., Anand, U., Oleksak, P., Tripathi, P., Lal, J. A., Thomas, G., . . . Tripathi, V. (2021). Novel CRISPR-Cas Systems: An Updated Review of the Current Achievements, Applications, and Future Research Perspectives. International journal of molecular sciences, 22(7), 3327. doi:10.3390/ijms22073327

NLRP5 NLR family pyrin domain containing 5 [homo sapiens (human)] - gene - NCBI. (January 5 2022). Retrieved from https://www.ncbi.nlm.nih.gov/gene/126206

Ringer, K. P., Roth, M. G., Garey, M. S., Piorczynski, T. B., Suli, A., Hansen, J. M., & Alder, J. K. (2018). Comparative analysis of lipid-mediated CRISPR-Cas9 genome editing techniques. Cell biology international, 42(7), 849-858. doi:10.1002/cbin.10952

Scheffner, M., & Whitaker, N. J. (2003). Human papillomavirus-induced carcinogenesis and the ubiquitin–proteasome system. Seminars in cancer biology, 13(1), 59-67. doi:10.1016/S1044-579X(02)00100-1

Scheffner, M., Huibregtse, J. M., Vierstra, R. D., & Howley, P. M. (1993). The HPV-16 E6 and E6-AP complex functions as a ubiquitin-protein ligase in the ubiquitination of p53. Cell, 75(3), 495-505. doi:https://doi.org/10.1016/0092-8674(93)90384-3

Seventh edition ed.). Philadelphia, PA: Lippincott Williams & Wilkins.

Smith, J. A., White, E. A., Sowa, M. E., Powell, M. L. C., Ottinger, M., Harper, J. W., & Howley, P. M. (2010). Genome-wide siRNA screen identifies SMCX, EP400, and Brd4 as E2-dependent regulators of human papillomavirus oncogene expression. Proceedings of the National Academy of Sciences, 107(8), 3752. doi:10.1073/pnas.0914818107

Sternberg, S. H., Redding, S., Jinek, M., Greene, E. C., & Doudna, J. A. (2014). DNA interrogation by the CRISPR RNA-guided endonuclease Cas9. Nature (London), 507(7490), 62-67. doi:10.1038/nature13011

The HPV Vaccine: Access and Use in the U.S. (2021). Retrieved from https://www.kff.org/womens-health-policy/fact-sheet/the-hpv-vaccine-access-and-use-in-the-u-s/

Toots, M., Ustav, J. M., Männik, A., Mumm, K., Tämm, K., Tamm, T., . . . Ustav, M. (2017). Identification of several high-risk HPV inhibitors and drug targets with a novel high-throughput screening assay. PLoS pathogens, 13(2), e1006168-e1006168. doi:10.1371/journal.ppat.1006168

Wang, F., Guo, T., Jiang, H., Li, R., Wang, T., Zeng, N., . . . Wang, Q. (2018). A comparison of CRISPR/Cas9 and siRNA-mediated ALDH2 gene silencing in human cell lines. Molecular Genetics and Genomics, 293(3), 769-783. doi:10.1007/s00438-018-1420-y

Wang, M., Zuris, J. A., Meng, F., Rees, H., Sun, S., Deng, P., . . . Xu, Q. (2016). Efficient delivery of genome-editing proteins using bioreducible lipid nanoparticles. Proceedings of the National Academy of Sciences, 113(11), 2868-2873. doi:10.1073/pnas.1520244113

Wang, T., Larcher, L. M., Ma, L., & Veedu, R. N. (2018). Systematic Screening of Commonly Used Commercial Transfection Reagents towards Efficient Transfection of Single-Stranded Oligonucleotides. Molecules (Basel, Switzerland), 23(10), 2564. doi:10.3390/molecules23102564

Wu, X., Mao, S., Ying, Y., Krueger, C. J., & Chen, A. K. (2019). Progress and Challenges for Live-cell Imaging of Genomic Loci Using CRISPR-based Platforms. Genomics, proteomics & bioinformatics, 17(2), 119-128. doi:10.1016/j.gpb.2018.10.001

Zhang, C., Zhao, X., Du, W., Shen, J., Li, S., Li, Z., . . . Liu, F. (2020). Ran promotes the proliferation and migration ability of head and neck squamous cell carcinoma cells. Pathology, research and practice, 216(6), 152951-152951. doi:10.1016/j.prp.2020.152951

Zhang, J. H., Chung, T. D., & Oldenburg, K. R. (1999). A Simple Statistical Parameter for Use in Evaluation and Validation of High Throughput Screening Assays. J Biomol Screen, 4(2), 67-73. doi:10.1177/108705719900400206